Cross regulation in a three-component cell envelope stress signaling system

Xingru Chen, Melene A. Alakavuklar, Aretha Fiebig, Sean Crosson

Department of Microbiology and Molecular Genetics, Michigan State University, East Lansing, MI, USA

Abstract

A multi-layered structure known as the cell envelope separates the controlled interior of bacterial cells from a fluctuating physical and chemical environment. The transcription of genes that determine cell envelope structure and function is commonly regulated by two-component signaling systems (TCS), comprising a sensor histidine kinase and a cognate response regulator. To discover TCS genes that contribute to cell envelope function in the intracellular mammalian pathogen, *Brucella ovis*, we subjected a comprehensive collection of non-essential TCS deletion mutants to compounds that disrupt cell membranes and the peptidoglycan cell wall. Our screen led to the discovery of three TCS proteins that coordinately function to confer resistance to cell envelope stressors and to support *B. ovis* replication in the intracellular niche. This tripartite regulatory system includes the conserved envelope regulator, CenR, and a previously uncharacterized TCS, EssR-EssS. The CenR and EssR response regulators bind a shared set of sites on the *B. ovis* chromosomes to control transcription of an overlapping set of genes with cell envelope functions. CenR directly interacts with EssR and functions to stimulate phosphoryl transfer from the EssS kinase to EssR and control steady-state levels of EssR protein in the cell. Our data provide evidence for a new mode of TCS cross-regulation in which a non-cognate response regulator regulates both activity and cellular levels of a cognate TCS protein pair.

Significance

Brucella species are the etiologic agents of brucellosis, a disease that inflicts a significant burden on global human health and agricultural production. As intracellular pathogens, *Brucella* must contend with a variety of host-derived stressors when infecting a host cell. The inner membrane, cell wall, and outer membrane — i.e. the cell envelope — of *Brucella* provides a critical barrier to host assault. A conserved regulatory mechanism known as two component signaling (TCS) commonly controls transcription of genes that determine the structure and biochemical composition of the cell envelope during stress. The importance of this study lies in the identification of previously uncharacterized TCS genes that determine *B. ovis* survival in the presence of cell envelope disruptors and within infected mammalian host cells. Our study has further uncovered a new molecular mechanism of TCS gene regulation, and thereby advances fundamental understanding of transcriptional regulatory processes in bacteria.

Introduction

Genes that regulate adaptation to changes in the physical and chemical state of the environment are important fitness determinants in bacteria (1-6). As intracellular pathogens, *Brucella* spp., inhabit the interior of mammalian cells and must adapt to numerous host-derived assaults including oxidative stress, nutrient limitation, and low pH. Accordingly, *Brucella* strains harboring mutations in genes that function to mitigate these stresses often have reduced fitness in the intracellular niche, e.g. (7-17). As in other bacteria, two-component signaling systems (TCS) are prominent regulators of *Brucella* stress responses (18, 19). Canonical two-component signaling entails signal-induced autophosphorylation of a sensor histidine kinase (HK), followed by specific phosphoryl transfer to a single DNA-binding response regulator (RR) protein that controls a transcriptional response (20). The vast majority of systems follow this classic paradigm, though there are examples of signal transduction processes that likely involve cross-regulation between otherwise distinct TCS protein pairs, e.g. (21-27).

A common function of TCS pathways is to regulate the biochemical composition and transport capacity of the cell envelope (28, 29), which serves as the barrier between the interior of the cell and the surrounding environment (30). As Gram-negative bacteria, the envelope of *Brucella* spp. contains two structurally distinct lipid bilayers with a thin periplasm and peptidoglycan cell wall in the space between. The ovine venereal pathogen, *Brucella ovis*, provides an interesting comparative model to

investigate genes that regulate molecular features of the *Brucella* cell envelope as it is one of two naturally "rough" strains among the classical *Brucella* species, and thus does not synthesize repeating O-polysaccharide units that extend from the core LPS oligosaccharide of the outer membrane (31). We sought to define the contribution of non-essential *B. ovis* TCS genes to cell survival under cell envelope stress conditions, with an additional goal of assessing functional relationships between TCS genes. To this end, we generated a collection of mutant strains harboring in-frame deletions of 32 non-essential TCS genes and measured growth/viability phenotypes of these strains on solid media containing sodium dodecyl sulfate (SDS) and carbenicillin, to target the cell membrane and cell wall, respectively. Five *B. ovis* TCS mutant strains were either more sensitive or more resistant than wild type (WT) to these specific cell envelope disruptors. Among these mutants, strains lacking the RR encoded by locus *BOV_1929* (BOV_RS09460; *cenR*) or the RR and HK encoded by locus *BOV_1472-73* (BOV_RS07250-55; *essR-essS*) had similar phenotypes under the tested conditions. Through a series of genetic, genomic, and biochemical experiments, we uncovered evidence for direct cross-regulation between these three TCS proteins, which control transcription of a common gene set to support *B. ovis* replication under *in vitro* envelope stress conditions and in the host intracellular niche. Specifically, the conserved alphaproteobacterial cell envelope regulator, CenR (32-34), both stimulates phosphoryl transfer between the cognate RR-HK pair, EssR-EssS, and regulates the steady-state levels of EssR in *B. ovis*. Our results expand understanding of molecular mechanisms of two-component signal transduction and define an unusual mode of TCS cross-regulation in *Brucella* that controls gene expression to enable stress resistance and intracellular replication.

Results

Tn-seq identifies a set of candidate essential TCS genes in Brucella ovis

There are 47 TCS genes in the *B. ovis* genome (Genbank accessions NC_009504 and NC_009505); four of these genes contain frameshift mutations and are defined as pseudogenes (Table S2). Several histidine kinases and response regulators are reported to be essential in *Brucella* spp. (35) and we sought to comprehensively define the essential set of TCS genes in *B. ovis* using *himar* transposon sequencing. Analysis of Tn-*himar* insertion sites in a collection of approximately 200,000 *B. ovis* mutants revealed ~54,000 unique TA dinucleotide insertions in the *B. ovis* genome (36). We used Hidden Markov Model and Bayesian-based approaches (37) to identify candidate essential genes based on this Tn-seq dataset (Table S1). As expected, many of the known TCS regulators of *Brucella* cell cycle and cell development (38) are defined essential using this approach including *ctrA*, *cckA*, *chpT*, *pdhS*, *divL*, and *divK*. Though insertion counts were lower in the developmental/cell cycle regulator *cpdR* relative to local background, this gene did not reach the essential threshold by our analysis. The *bvrS-bvrR* two-component system, which is homologous to the *chvG-chvI* system of other Alphaproteobacteria (39), is also essential. This result is consistent with a report by Martín-Martín and colleagues that the *bvrSR* genes cannot not be deleted in *B. ovis* (40). Notably, the *bvrSR* system is not essential in the smooth strains, *B. melitensis* (39), *B. abortus* (41). Finally, the *ntrX* regulator is also essential. Considering a recent report of strong genetic interactions between *ntrX*, *chvG*, and *chvI* in *Caulobacter* (42), the essential phenotypes of *bvrS-bvrR* and *ntrX* may be related.

TCS mutants sensitive (and resistant) to cell envelope disruptors in vitro

We next generated 24 mutant strains harboring in-frame deletions of 32 non-essential TCS genes in *B. ovis* (Table S2). In cases where sensor kinase and response regulator genes are adjacent in the *B. ovis* genome, we inferred that these genes functioned together and therefore deleted both. The double deletion strains include: Δ*BOV_0603-0604* (*feuPQ),* Δ*BOV_0611-0612*, Δ*BOV_1472-1473*, Δ*BOV_1075-1076* (*ntrCB*)*,* Δ*BOV_A0037-A0038* (*nodVW*), Δ*BOV_A209-A210,* Δ*BOV_0357-0358,* and Δ*BOV_A0412-A0413.* To identify TCS genes that function to regulate the cell envelope, we subjected the collection of non-essential deletion mutants to treatments known to compromise envelope integrity. Specifically, WT and *B. ovis* mutant strains were serially diluted and plated on plain tryptic soy agar supplemented with 5% sheep blood (TSAB) and on TSAB containing *a)* the detergent sodium dodecyl sulfate (SDS) or *b)* the cell wall targeting (beta-lactam) antibiotic carbenicillin. Five of the 24 mutant strains showed a growth or viability phenotype that differed from WT in multiple conditions including

Δ*BOV_0577 (divJ)*, Δ*BOV_1602*, Δ*BOV_1929*, Δ*BOV_0611-0612*, and Δ*BOV_1472-1473* (Figures 1 and S1).

All five mutants with envelope stress defects had reduced viability on TSAB containing 2 μg/ml carbenicillin relative to WT (Figure 1 and Figure S1), though the carbenicillin sensitivity phenotype of Δ*BOV_1602* was less severe than other strains (Figure 1A). The Δ*BOV_1929* single mutant and Δ*BOV_1472-1473* double mutant had a growth defect on TSAB, as evidenced by smaller colony size (Figure 1B and Figure S1B). Growth of WT *B. ovis* was impaired on TSAB containing 0.004% SDS, but the viability of Δ*BOV_1929* and Δ*BOV_1472-1473* was even more severely impacted under this condition (Figure 1B). Conversely, deletion of *BOV_1602*, a soluble cytoplasmic HWE family histidine kinase (43) containing an amino-terminal PAS domain (44), strongly enhanced *B. ovis* viability on SDS plates: visible growth was apparent in titers approximately three $\log_{10}$ units more diluted than WT (Figure 1A). *BOV_1602* is adjacent to the *nepR-ecfG-phyR* general stress response (GSR) locus (8) in *B. ovis*. It was reported that orthologs of this gene do not regulate *Brucella* spp. GSR *in vitro* or *in vivo* (7, 45), but control of the GSR system and σ^{EcfG}-dependent transcription is complex (2) and may involve *BOV_1602* under select conditions. In all cases, the observed agar plate phenotypes were genetically complemented by integration of a single copy of the deleted gene(s) with their native promoter at the *glmS* locus (Figure 1 and Figure S1A).

***A genetic connection between BOV_1472-1473* (*essRS) and BOV_1929* (*cenR*)**

There was notable congruence in the agar plate growth defects of the Δ*BOV_1929* and Δ*BOV_1472-1473* strains across the tested conditions, though Δ*BOV_1929* was more sensitive to carbenicillin than Δ*BOV_1472-1473* (Figure 1B). BOV_1929 has high sequence identity to CenR, which is a known regulator of cell envelope structure in the Alphaproteobacteria (33, 34): *BOV_1929* and *Caulobacter crescentus*, *Rhodobacter sphaeroides*, and *Sinorhizobium meliloti* CenR are reciprocal top-hit BLAST pairs (identity ranging from 65-80% over the full length of the protein). We have thus named *BOV_1929*, *cenR*. Consistent with our data, *Brucella melitensis cenR* (also known as *otpR*) has a reported role in beta-lactam tolerance (46) and acid stress response (47). Studies in *C. crescentus* and *R. sphaeroides* have identified the histidine kinase CenK as the cognate regulator of CenR (33, 34), but the *B. ovis* genome does not encode proteins with high sequence identity to *Caulobacter* or *Rhodobacter* CenK. This result agrees with a previous report that *B. melitensis* does not have an evident CenK ortholog (48). The *B. ovis* sensor kinase most closely related to *C. crescentus* and *R. sphaeroides* CenK is encoded by gene locus *BOV_0289* (33-37% amino acid identity), but the phenotypes of a Δ*BOV_0289* in-frame deletion mutant were the same as WT in the tested conditions. Furthermore, a Δ*BOV_0289* Δ*cenR* double mutant phenocopied the Δ*cenR* single mutant (Figure 1B). We conclude that the histidine kinase BOV_0289 does not function with CenR under the tested conditions.

Given the **e**nvelope **s**tress **s**urvival phenotypes of the Δ*BOV_1472-1473* double deletion mutant, we hereafter refer to the DNA-binding response regulator gene *BOV_1472* as *essR* and the sensor histidine kinase gene *BOV_1473* as *essS*. To our knowledge, EssS and EssR have not been functionally characterized, though EssS is 68% identical to the RL3453 sensor kinase that has been functionally linked to *Rhizobium leguminosarum* attachment to legume roots (49). EssR is an OmpR family response regulator, while the EssS sensor kinase has two predicted transmembrane helices and primary structure features that resemble the well-studied CpxA and EnvZ cell envelope regulators (50-52). To assess phenotypic relationships between the Δ*essR-essS* and Δ*cenR* mutants, we generated *B. ovis* strains harboring in-frame deletions of either *essR* or *essS* (Δ*essR*; Δ*essS*) and a Δ*cenR* Δ*essR-essS* triple mutant and plated these strains on TSAB containing SDS or carbenicillin as above. The Δ*essR* strain phenocopied the Δ*essR-essS* double mutant; the Δ*essS* phenotype was indistinguishable from WT on plain TSAB and TSAB-SDS but showed an intermediate carbenicillin sensitivity phenotype. The Δ*cenR* Δ*essR-essS* triple mutant phenocopied the Δ*cenR* and Δ*essR* single mutants (Figure 1B). These results provide evidence that CenR and EssR function in the same pathway; the function of *essS* in this pathway is unclear from these data. We note that sequence relatedness of *essR* and *cenR* is low (32% identity and 50% similarity) relative to all possible *B. ovis* response regulator pairings, though select regions of primary structure are conserved (Figure S1B), which will be discussed below.

Contribution of the CenR and EssR aspartyl phosphorylation sites to stress survival

CenR and EssR are both DNA-binding response regulator proteins, which are typically regulated by phosphorylation at a conserved aspartic acid residue in the receiver domain. To assess the functional role of the CenR aspartyl phosphorylation site (D55), we tested whether expression of non-phosphorylatable (*cenR*$_{D55A}$) or putative phosphomimetic (*cenR*$_{D55E}$) alleles of *cenR* genetically complemented the agar plate stress defects of a Δ*cenR* strain. Both mutant alleles of *cenR* restored Δ*cenR* growth/survival to WT levels, indicating that the CenR phosphorylation site does not impact CenR function under the assayed stress conditions (Figure 2). We conducted the same experiment for EssR, testing whether *essR*$_{D64E}$ and *essR*$_{D64A}$ could genetically complement the TSAB plate stress phenotypes of Δ*essR*. *essR*$_{D64E}$ complemented the defect of Δ*essR* on plain TSAB and TSAB-SDS plates but resulted in a strain that was more sensitive than Δ*essR* to carbenicillin. Expression of *essR*$_{D64A}$ failed to complement Δ*essR* under all conditions (Figure 2). From these results, we conclude that EssR phosphorylation at D64 contributes to *in vitro* stress survival of *B. ovis*.

***cenR* and *essR* mutants have equivalent cell size defects**

Previous studies of CenR in *C. crescentus* and *R. sphaeroides* have shown that depletion or overexpression of *cenR* leads to large defects in cell envelope structure and/or cell division (33, 34). Considering these results and the sensitivity of *B. ovis* Δ*cenR* to SDS and carbenicillin, we inspected Δ*cenR,* Δ*essR*, and Δ*essS* cells by phase contrast light microscopy and cyro-electron microscopy for defects in cell envelope structure or cell morphology. Deletion of *cenR*, *essR* or *essS* did not result in apparent changes in cell morphology or cell division as assessed by phase contrast microscopy at 630x magnification (Figure S2A). However, an analysis of cell size revealed that both Δ*cenR* and Δ*essR* mutant cells had ~12% larger cell area than WT ($p<0.0001$) (Figure S2B). Again, the parallel phenotype of Δ*cenR* and Δ*essR* supports a model in which these two genes execute related functions. An intact phosphorylation site was not required for CenR or EssR to affect cell size, as expression of either phosphorylation site mutant allele of *cenR*(D55) or *essR*(D64) restored cell size to WT levels (Figure S2B). We did not observe major cell membrane defects in Δ*cenR* and Δ*essR* mutant cells by cryo-EM (Figure S2C). We conclude that the SDS and carbenicillin resistance defects we observe in the Δ*cenR* and Δ*essR* strains are associated with a defect in cell size control.

B. ovis* Δ*cenR*, Δ*essR*, and Δ*essS* strains have equivalent fitness defects in a macrophage infection model

The *in vitro* phenotypic data for *essS*, *essR*, and *cenR* mutants failed to clearly identify a kinase that may regulate EssR and/or CenR. This result motivated us to test the phenotypes of these TCS mutant strains in a cell-based infection model. As *B. ovis* is an intracellular pathogen, a cell-based infection system more closely models stress conditions encountered by the bacterium in natural settings. Δ*cenR,* Δ*essR*, and Δ*essS* strains had no defect shortly after entry (2h post-infection) or at early stages of infection (6h & 24h p.i.) of THP-1 macrophage-like cells relative to WT. By 48h p.i., recoverable CFU of WT *B. ovis* increased, consistent with adaptation and replication in the intracellular niche; CFU of Δ*cenR,* Δ*essR*, and Δ*essS* did not increase appreciably between 24 and 48h. The 1 $\log_{10}$ unit intracellular replication defect of the Δ*cenR,* Δ*essR*, and Δ*essS* strains at 48h was complemented by expression of the deleted gene(s) from an ectopic locus (Figure 3). Thus, loss of *cenR, essR*, or *essS* does not affect macrophage entry or early survival but does affect replication and/or survival after 24h. These results indicate that *essS*, *essR*, and *cenR* contribute to *B. ovis* fitness after the establishment of the replicative niche inside the *Brucella*-containing vacuole, and that EssS functions with EssR when *B. ovis* encounters stresses in the host intracellular environment.

Additionally, we tested the infection phenotypes of strains harboring alleles of *essR* and *cenR* in which the conserved aspartyl phosphorylation site was mutated. Expression of *cenR*$_{D55A}$ or *cenR*$_{D55E}$ partially - and equivalently - complemented the infection defect of Δ*cenR* (Figure 3A). Expression of *essR*$_{D64E}$ and *essR*$_{D64A}$ both failed to complement Δ*essR* (Figure 3B). We conclude that an intact aspartyl phosphorylation site in both the CenR and EssR receiver domains is required for WT levels of replication in a THP-1 macrophage infection model.

EssR and CenR regulate a common gene set

Genetic data presented to this point provide evidence that the EssR-EssS two-component system and the response regulator CenR have related functional roles in regulation of *B. ovis* cell envelope biology and intracellular replication. Considering that TCS proteins typically function to regulate transcription, we used RNA sequencing (RNA-seq) to assess the relationship between EssRS- and CenR-regulated gene sets. The global transcriptional profiles of Δ*cenR* and Δ*essRS* mutant strains were highly correlated (Figure 4). Filtering genes based on a minimum fold change ≥ |2| (FDR p-value < 10^{-4}) revealed 53 genes regulated by *essR-essS* and 61 genes regulated by *cenR* (Figure 4; Table S3). Thirty-eight (38) of these genes are regulated in the same direction in both datasets, indicating a high degree of functional overlap of EssRS and CenR, with respect to gene expression. With few exceptions, genes that met the criteria for regulation in only one strain were still regulated in the other strain but at a lower significance level. One potential explanation for the observed regulatory overlap is that EssR and CenR transcription depend on each other. However, transcript levels of *essR-essS* in a Δ*cenR* background, and *cenR* in Δ*essR-essS* background do not differ significantly from WT (Table S3). CenR and EssR therefore do not regulate each other at the transcriptional level. Rather, CenR and EssR either independently or coordinately regulate transcription of an overlapping set of *B. ovis* genes.

To further investigate the connection between CenR- and EssR-dependent transcription, we performed chromatin-immunoprecipitation (ChIP)-seq with both EssR and CenR. To promote RR binding to chromosomal target sites, we expressed putative phosphomimetic alleles (D→E) of each RR from their native promoters integrated at the *glmS* locus in each mutant strain; genes were fused to a C-terminal 3xFLAG tag. ChIP of $EssR_{D64E}$-3xFLAG yielded 65 significant peaks across two biological replicates, and ChIP of $CenR_{D55E}$-3xFLAG yielded 47 significant peaks across three biological replicates. Thirty-three peaks were shared between $CenR_{D55E}$ and $EssR_{D64E}$ (Figure 4B and Table S4) providing additional support for a model in which CenR and EssR regulate transcription of a shared gene set, functioning either separately or as a heteromeric complex.

Genes with cell envelope functions are abundant in the CenR-EssRS regulon

The gene with the largest differential expression in both Δ*cenR* and Δ*essRS* RNA-seq datasets was *BOV_1399*, which encodes a predicted periplasmic protein related to soluble lytic murein transglycosylase (SLT) enzymes (Conserved Domain Database e-value < 10^{-25}). In both datasets *BOV_1399* transcript levels decreased ≈ 48-fold (Figure 4; Table S3). To test if the loss of BOV_1399 expression could explain the stress survival phenotypes we observed in the mutant strains, we deleted *BOV_1399* and subjected this mutant to the same agar plate growth assays described above. However, the phenotypes of Δ*BOV_1399* in these assays were indistinguishable from WT.

Genes encoding membrane transport proteins are highly represented in the regulon(s). Thirteen membrane transport related proteins are present in the CenR/EssR regulon, and nine clusters of genes positioned adjacently on the *B. ovis* chromosomes are co-regulated (Figure 4). The largest cluster of adjacent genes in the *cenR* and *essR* regulon is on chromosome 2 and encodes predicted carbohydrate metabolism (*BOV_A0354-A0355*) and transport genes (*BOV_A0347-A0348*; *BOV_A0350-A0352*), a DapA-family dihydrodipicolinate synthase/N-acetylneuraminate lyase (*BOV_0349*), and two Gfo/Idh/MocA family oxidoreductases (*BOV_A0345-A0346*); all are significantly decreased upon *cenR* or *essRS* deletion (Figure 4; Table S3). It is notable that homologs of genes in this cluster are also regulated by CenR in *R. sphaeroides* based on data of Lakey et al. (33) (Table S3). Expression of a third Gfo/Idh/MocA family oxidoreductase (*BOV_0234*) is also decreased in both deletion strains as is the secreted protein BA14K (*BOV_A0688*), which is required for normal spleen colonization in a mouse model of *B. abortus* infection (8). Transcripts of three genes immediately adjacent to the general stress response regulator, PhyR, are decreased upon *cenR* or *essRS* deletion, including the PAS HWE-family sensor kinase *BOV_1602* described in sections above (Figure 4). Additionally, transcripts of the predicted sulfate ABC transport operon, *cysWTP*, decreased significantly in both deletion mutant strains (Figure 4A; Table S3).

Nine genes have significantly higher expression in Δ*cenR* and Δ*essRS* (Table S3 and S4) including a site-specific DNA integrase (*BOV_0631*), an ABC transporter protein (*BOV_A0247*), a

predicted membrane-bound inhibitor of C-type lysozyme (*BOV_0447*) and LysM-domain protein (*BOV_0448*), the envelope integrity protein B gene (*eipB*; *BOV_1121*), and a CREC-EF hand family protein (*BOV_1296*) that is reported to be directly regulated by the virulence regulator VjbR under select conditions (53). The contributions of these regulated genes to the Δ*cenR* and Δ*essRS* envelope stress and infection phenotypes remain to be determined.

CenR and EssR physically interact via their REC domains in a heterologous system

Genetic, transcriptomic, and ChIP-seq data all indicate that the response regulators EssR and CenR directly control expression of a common gene set in *B. ovis* to enable growth in the presence of SDS and carbenicillin. While the molecular processes that determine signaling via a particular TCS pathway are typically insulated from other TCS proteins (20), we postulated that the congruent genetic and molecular phenotypes of Δ*cenR* and Δ*essR* strains could arise through direct molecular interactions of CenR with either EssS, EssR, or both. In fact, in a systematic analysis of *B. abortus* TCS protein interactions, Hallez and colleagues previously reported the surprising observation that EssR (then, generically annotated as TcbR) and CenR interact in a yeast two-hybrid assay (54). EssR and CenR were the only two *B. abortus* RRs that showed interaction in their genome-scale screen. To test EssR and CenR protein-protein interaction in a heterologous system, we used a bacterial two-hybrid approach based on the T18 and T25 domains of the split adenylate cyclase enzyme (55). CenR and EssR showed strong interactions when fused to either adenylate cyclase domain, while the homomeric CenR-CenR and EssR-EssR combinations showed no evidence of interaction (Figure 5A).

To test the contribution of the conserved aspartyl phosphorylation sites of CenR and EssR to the observed two-hybrid interaction, we fused putative phosphomimetic (D→E) or non-phosphorylatable (D→A) alleles of either CenR or EssR to the T18 and T25 fragments of adenylate cyclase. Both $EssR_{D64A}$ and $EssR_{D64E}$ interacted with CenR to the same extent as WT EssR (Figure 5B). $CenR_{D55E}$ had significantly reduced interaction with EssR, while $CenR_{D55A}$ interaction with EssR was not significantly different. These results provide evidence that CenR phosphorylation attenuates its interaction with EssR. Homomeric CenR-CenR or EssR-EssR interactions were again not observed in our two-hybrid assay for either the D→A or D→E mutants (Figure 5B).

We used the neural network models of AlphaFold2 (56), as implemented in AF2Complex (57), to develop hypotheses about the structural basis of CenR-EssR interaction. The results of this computation predicted that these two response regulators interact primarily through their receiver (REC) domains rather than their DNA-binding (DBD) domains (Figure 5C). Predicted (1:1) CenR:EssR complex structures showed parallel REC domain heterodimers with significant buried surface area in a region of homologous primary structure of CenR and EssR (Figure S1). To test if CenR and EssR interact via their REC domains, we again used a bacterial two-hybrid assay. The measured interaction of the isolated CenR and EssR REC domains was comparable to that of the full-length proteins (Figure 5D). None of the other DBD-DBD or DBD-REC combinations had significant interactions.

CenR-EssR interaction in B. ovis

Given the result that CenR and EssR strongly interact via their REC domains in a heterologous system, we sought to test whether these two proteins interact in *B. ovis* cells by co-immunoprecipitation. Briefly, we expressed a *cenR-3xFLAG* fusion from the native *cenR* promoter on a low-copy plasmid in either strains lacking endogenous CenR (Δ*cenR*) or lacking both response regulators (Δ*cenR* Δ*essR*) and applied the crosslinked lysates to anti-FLAG magnetic beads. After multiple washing steps we eluted bound protein, reversed the crosslinks, and resolved the eluate by SDS-PAGE. Western blot using polyclonal EssR antiserum revealed clear EssR bands in the lysates of both Δ*cenR / cenR-3xFLAG* and Δ*cenR* vector control strains, but not in Δ*cenR* Δ*essR / cenR-3xFLAG*. Among the three eluate fractions, only the strain expressing *cenR-3xFLAG* yielded a strong EssR band on the Western blot (Figure 5E). These results provide evidence that the CenR-EssR interaction demonstrated by bacterial two-hybrid assay occurs in *B. ovis* cells.

CenR enhances the rate of EssS-EssR phosphoryl transfer

The related phenotypes of *cenR* and *essR* mutants and the fact that these two response regulators physically interact in cells raised questions about the biochemical consequence(s) of EssR/CenR interaction on histidine kinase autophosphorylation and phosphoryl transfer. The data presented to this point do not clearly establish the identity of a sensor kinase in this system, though we considered EssS to be a strong candidate. To test this hypothesis, the cytoplasmic kinase domain of EssS (aa 191-488) and full-length EssR and CenR response regulators were purified. The EssS kinase domain autophosphorylated *in vitro*; incubating EssS kinase domain with EssR resulted in rapid loss of phospho-EssS (EssS~P) signal and a concomitant increase in phospho-EssR (EssR~P) signal within 30s, indicating phosphoryl transfer (Figure 6A). Incubation of EssS with CenR resulted in no detectable phosphoryl transfer by 600s, even when CenR was added in 50 molar excess. We conclude that EssS is the cognate kinase for EssR, and that EssS does not directly phosphorylate CenR.

Though EssS does not phosphorylate CenR *in vitro*, we postulated that CenR may influence activity of the EssS-EssR TCS in some way. To test this idea, we first mixed equimolar EssS and EssR with increasing concentrations of CenR. Supplementing an EssS-EssR reaction mixture with CenR at a 1:1:1 molar ratio resulted in a ~20% reduction of EssS-P levels after 20s relative to a 1:1 EssS-EssR reaction (Figure S3). Adding CenR to the reaction mixture at 5x molar excess (1:1:5), resulted in 40% reduction of EssS-P relative to a 1:1 EssS-EssR reaction at 20s. The effect of CenR addition on EssS~P levels (at 20 s) saturated at a 1:1:5 ratio (Figure S3). To further investigate the effect of CenR on the EssS-EssR system, we conducted kinetic measurements of EssS to EssR phosphoryl transfer by measuring both EssS~P and EssR~P signal over a 1-minute time course. EssS to EssR phosphoryl transfer reactions containing 5-molar excess CenR had an enhanced rate of (apparent) EssR~P production and an enhanced rate of EssS~P loss compared to reactions with EssS and EssR only (Figure 6D); we note these experiments do not rule out the possibility that CenR is phosphorylated by EssS when EssR is present. Steady-state levels of the gel band we attribute to EssR~P are maximal by 15s when 5x CenR is present. These experiments provide evidence that CenR stimulates phosphoryl transfer from EssS to EssR.

***cenR* and *essS* influence steady-state EssR protein levels**

Stimulation of EssS to EssR phosphoryl transfer by the non-cognate CenR protein provides one explanation for the related phenotypes of the Δ*cenR*, Δ*essS* and Δ*essR* mutants. We sought to test whether the CenR protein may have other regulatory effects on the cognate EssS-EssR TCS pair in *B. ovis*. EssR and CenR do not regulate each other's transcription (Table S3) but, considering these two proteins physically interact, we hypothesized that CenR could impact steady-state EssR protein levels through a post-transcriptional mechanism. To test this hypothesis, we measured EssR protein by Western blot in WT and Δ*cenR*. Deletion of *cenR* resulted in a significant reduction (~70%) of EssR protein levels. The Δ*essS* strain also had significantly reduced EssR levels, though the effect was not as large as Δ*cenR* (Figure 7). The effect of EssS on EssR protein levels was not apparently a result of EssR phosphorylation as steady-state levels of EssR, EssR(D64A) and EssR(D64E) did not differ significantly. The direct impact of CenR-EssR interaction on EssR protein stability remains undetermined, but reduced EssR levels in a Δ*cenR* background provide an additional explanation of the phenotypic congruence of Δ*cenR* and Δ*essR*. The intermediate level of EssR protein in the Δ*essS* strain is consistent with the intermediate phenotype of this mutant in agar plate growth assays.

Discussion

Multiple TCS genes are typically present in bacterial genomes, and the proteins they encode most often function separately to regulate distinct transcriptional responses (20). Our systematic analysis of *B. ovis* TCS genes revealed two DNA-binding response regulators, *cenR* and *essR*, that had related morphological, stress resistance, and infection phenotypes when deleted. These results informed the hypothesis that CenR and EssR work together to execute their functions in the cell and led to the discovery of a new cell envelope regulatory system (EssS-EssR) and a new mechanism of TCS regulation in bacteria that we discuss below.

Discovery of a cell envelope regulatory system in *Brucella*

TCS proteins play a key role in the regulation of cell envelope biogenesis and homeostasis in the bacterial kingdom (29, 58, 59). The function of the EssR-EssS TCS protein pair has not been defined in any species prior to this study, and our data provide evidence that these two proteins play an important role in *Brucella* resistance to cell envelope disruptors *in vitro*, and in regulating processes important for intracellular replication in a macrophage model. Apparent orthologs of the sensor kinase, EssS (>70% identity over the full length of protein), are present in select genera across the order *Hyphomicrobiales* including *Brucella*, *Mesorhizobium*, *Rhizobium*, *Phyllobacterium*, *Bartonella*, and *Hoeflea*; EssR has a similar phylogenetic distribution. Though the HK domain of EssS has low sequence identity to the HK domains of well-described Gram-negative envelope regulators such as CpxA and EnvZ (30-35%), multiple sequence alignment models in the conserved domain database (CDD) (50) indicate that EssS, CpxA, and EnvZ have common ancestry (e-value < 10^{-40}). Likewise, EssR is most closely related to the OmpR sequence family in the CDD (e-value < 10^{-70}). OmpR functions as the cognate regulator of the EnvZ kinase in enteric bacteria.

EssS and EssR clearly form a cognate signaling pair *in vitro* as evidenced by specific phosphoryl transfer from the EssS kinase domain to EssR on a fast time scale (Figure 6). However, the phenotypes of the Δ*essS* and Δ*essR* strains are not equivalent in an *in vitro* model of cell envelope stress. Specifically, *essR* deletion results in large growth defects on agar when the mutant is challenged with SDS and carbenicillin; deletion of *essS* has no apparent consequence under SDS challenge and the carbenicillin phenotype is less severe than Δ*essR* (Figure 1B). However, the phenotypes of Δ*essS* and Δ*essR* are equivalent in a macrophage infection model. Neither of these mutants have an entry defect, but both fail to initiate robust replication ~24 hours after infection (Figure 3). This result provides evidence that EssS-dependent phosphorylation (or dephosphorylation) of EssR is more important for system function in the complex environment of the intracellular niche than it is in a simple *in vitro* agar plate assay. It is also evident from our data that the non-cognate regulator, CenR, directly regulates activity of the cognate EssR-EssS system, though the contribution of CenR phosphorylation to this process is not presently known.

An unexpected functional role for the conserved cell envelope regulator, CenR

The result that *B. ovis* CenR confers resistance to SDS and carbenicillin (Figures 1 & 2) was not unexpected considering the phenotypes of *cenR* mutants in other Alphaproteobacteria. CenR was first described as an essential RR in *C. crescentus*, where it functions to regulate cell envelope structure (34), and is now known to be conserved in many alphaproteobacterial orders (33). Recent work has shown *cenR* to be essential in *R. sphaeroides*, where it controls transcription of the Tol-Pal outer membrane complex and other cell envelope genes (33), and in *Sinorhizobium meliloti* where it mediates osmotolerance and oxidative stress resistance (32). In all three of these species, CenR is regulated by a cognate histidine kinase, CenK. Our data show that *cenR* is not essential for *B. ovis* growth or division under standard culture conditions and indicate that it is an orphan response regulator, which is consistent with a report from Zhang et al. in *B. melitensis* (48). The possibility that a *Brucella* HK phosphorylates (or dephosphorylates) CenR under certain conditions cannot be conclusively ruled out from our data. Indeed, there is some evidence that the conserved CenR aspartyl phosphorylation site can impact CenR-EssR interaction (Figure 5) and replication in the intracellular niche (Figure 3). Nonetheless, both $cenR_{D55A}$ and $cenR_{D55E}$ alleles fully complement the agar plate stress phenotypes of Δ*cenR*. And unlike *R. sphaeroides* and *C. crescentus*, where *cenR* depletion results in major defects in cell envelope structure, the impact of *cenR* deletion on *B. ovis* cell morphology is small: *B. ovis* Δ*cenR* mutants are slightly (but significantly) larger than WT (Figure S2), but the morphology of the mutant cells otherwise appears normal. These results indicate that CenR function in *Brucella* differs from *Caulobacter*, *Rhodobacter*, and *Sinorhizobium*.

CenR is a post-transcriptional regulator of the EssS-EssR two-component system

Cross-regulation between TCSs is uncommon, though there is experimental support for direct interactions between otherwise distinct TCS HK-RR protein pairs for limited number of systems. For example, the NarXL and NarQP systems of *Escherichia coli* cross-phosphorylate to tune nitrate and nitrite respiratory processes (60), and in *C. crescentus*, a consortium of sensor kinases that coordinately

regulate cell adhesion in response to a range of environmental cues physically interact in cells (23). In this manuscript, we present evidence for a mode of TCS cross-regulation in which a non-cognate RR (CenR) directly stimulates the phosphoryl transfer activity of a cognate HK-RR protein pair (EssS-EssR) (Figure 6). We further demonstrate that CenR ensures normal levels of EssR protein in *Brucella* cells via a post-transcriptional mechanism. Specifically, deletion of *cenR* does not impact *essR* transcript levels, but results in a 70% reduction in EssR protein (Figure 7). EssR and CenR physically interact via their receiver domains (Figure 5), and it seems most likely that CenR protects EssR from proteolytic degradation in cells though we cannot rule out other post-transcriptional models at this time. The positive effect of CenR on EssS-EssR phosphoryl transfer activity and on EssR protein levels are consistent with the phenotypes of strains lacking *cenR* and *essR*.

However, CenR does not simply control the activity and levels EssS-EssR. CenR is itself a DNA binding protein, and we have presented evidence that EssR and CenR both directly and indirectly regulate transcription of a highly correlated set of genes that includes multiple transporters and cell wall metabolism genes (Figure 4). These two transcriptional regulators directly bind shared and unique sets of sites on *B. ovis* chromosomes 1 and 2. It is possible that CenR and EssR bind DNA as heterodimers, which has been described for the BldM and WhiI response regulators of *Streptomyces* (61), and the RcsB regulator of *E. coli* with GadE (62) and BglJ (63). These heterodimeric regulators are competent to control different classes of promoters depending on oligomeric state; a similar mechanism may exist for EssR and CenR though we have not identified distinct promoter classes in our data. It is plausible that CenR and EssR bind as homodimers and heterodimers considering the pattern of unique and overlapping genes/promoters in the transcriptomic and ChIP-seq datasets. Future studies aimed at deciphering molecular features of environmental signal detection by the EssS sensor kinase, allosteric regulation of TCS activity by CenR, and transcriptional control by the CenR and EssR regulators will generally inform our understanding of the evolution of cell envelope regulatory systems in bacteria. More specifically, investigation of these proteins will illuminate mechanisms by which *Brucella* replicate in the intracellular niche and spread from cell to cell in face of harsh immune stresses encountered within the host.

Materials and Methods

Bacterial strains and growth conditions

All *Brucella ovis* strains were grown on Tryptic soy agar (BD Difco) + 5% sheep blood (Quad Five) (TSAB) or in Brucella broth at 37˚C with 5% CO_2 supplementation. Growth medium was supplemented with 50 µg/ml kanamycin, 30 µg/ml oxytetracycline, 2 µg/ml carbenicillin, or 0.004% sodium dodecyl sulfate (SDS) when necessary.

All *Escherichia coli* strains were grown in lysogeny broth (LB) or on LB solidified with 1.5% w/v agar. *E. coli* Top10 and WM3064 strains were incubated at 37˚C and BTH101 strains were incubated at 30˚C. WM3064 was grown with 30 µM diaminopimelic acid (DAP) supplementation. Medium was supplemented with 50 µg/ml kanamycin, 12 µg/ml oxytetracycline or 100 µg/ml carbenicillin when necessary. Primer, plasmid, and strain information are available in Table S5.

Essential gene calculations using *B. ovis* Tn-himar sequencing data

We constructed a library of *B. ovis* transposon mutants as described previously (15). Briefly, the *E. coli* strain APA752, harboring the pKMW3 mariner transposon library, was conjugated into WT *B. ovis* and transposon bearing strains were selected on TSAB supplemented with 50 µg/ml kanamycin. Following an outgrowth of pooled mutants in 250 ml Brucella broth to $OD_{600} \approx 0.6$, cells were frozen in 25% glycerol in 1 ml aliquots. An aliquot was thawed for gDNA extraction and subsequent insertion site mapping, as described (64). The library contained insertions at over 50,000 unique sites in the genome. Insertion site sequencing data is available in the NCBI sequence read archive under accession SRR19632676. Using the insertion site mapping data from this Tn-seq dataset, we applied the HMM and Gumbel algorithms in the TRANSIT (37) software package to identify candidate essential genes (see Table S1).

Chromosomal deletion strain construction

The double-crossover recombination method was used to generate all *B. ovis* strains bearing in-frame, unmarked gene deletions. Approximately 500 base pair (bp) upstream or downstream of the target gene, including 9-120 bp of the 3' and 5' ends of the target gene, were amplified by PCR using KOD Xtreme polymerase (Novagen) using primers (Table S5) specific to these regions and the *B. ovis* genomic DNA as template. The DNA fragments were then inserted into the *sacB*-containing suicide plasmid pNPTS138 either through Gibson assembly or restriction enzyme digestion and ligation. The ligated plasmids were first chemically transformed into competent *E. coli* Top10. After sequencing confirmation, plasmids were transformed into chemically competent *E. coli* WM3064 (strain originally produced by W. Metcalf), a DAP auxotroph conjugation-competent donor strain. Plasmids were transferred to *B. ovis* through conjugation. Primary recombinants were selected on TSAB supplemented with kanamycin. After outgrowth in non-selective growth in Brucella broth for 8 hours, clones in which a second recombination removed the plasmid were identified through counter selection with 5% sucrose. Colony PCR was performed on kanamycin-sensitive colonies to distinguish clones bearing the deletion allele from those bearing the WT allele.

Complementation strain construction

To engineer genetic complementation constructs, target genes were amplified by KOD polymerase, including ~300 bp upstream and ~50 bp downstream of each target gene. The PCR products were purified and inserted into plasmid pUC18-mTn7 by restriction enzyme digestion and ligation, followed by chemical transformation into *E. coli* TOP10 cells. After sequence confirmation, the mTn7 plasmids were transformed into chemically competent *E. coli* WM3064. These plasmids were co-conjugated into *B. ovis* strains with a Tn7 integrase expressing suicide helper plasmid, pTNS3, which is also carried by WM3064. *B. ovis* colonies carrying the integrated mTn7 constructs at the *glmS* locus were selected on TSAB containing kanamycin.

Agar plate growth/stress assays

After 2 days of growth on TSAB or TSAB supplemented with kanamycin, *B. ovis* cells were collected and resuspended in sterile phosphate-buffered saline (PBS) to an OD_{600} = 0.3. Each strain was serially diluted in PBS using a 10^{-1} dilution factor. 5 µl of each dilution was plated onto either TSAB, TSAB containing 0.004% SDS, or 2 µg/ml carbenicillin. After 3 days of incubation for TSAB, 4 days for TSAB + 0.004% SDS and 5 days for TSAB + 2 µg/ml carbenicillin, growth was documented photographically.

Macrophage infection assay

THP-1 cells were grown in Roswell Park Memorial Institute Medium (RPMI) + 10% heat inactivated fetal bovine serum (FBS) at 37˚C with 5% CO_2 supplementation. Three days prior to infection, THP-1 cells were seeded in a 96-well plate at a concentration of 10^6 cells/ml in 100 µl/well of fresh RPMI + 10% FBS with an addition of 50ng/ml phorbol 12-myristate-13-acetate (PMA) to induce differentiation. After three days at 37˚C in 5% CO_2, *B. ovis* cells were resuspended at a concentration of 10^8 CFU/ml (OD_{600} = 0.15) in RPMI + 10% FBS and added to THP-1 cells at a multiplicity of infection (MOI) of 100. The 96-well plate containing *B. ovis* and THP-1 cells was centrifuged at 150 x g at room temperature for 5 minutes and incubated at 37˚C with 5% CO_2 for 1h. Media was removed and fresh media containing 50 µg/ml gentamicin was added to kill extracellular *B. ovis* that were not internalized. The plate was incubated for another hour at 37˚C with 5% CO_2. Media was removed and fresh media containing 25 µg/ml gentamicin was added to each well except for 2h-p.i. wells. A 2h, 6h, 24h, and 48h post-infection, *B. ovis* were enumerated by removing the media and washing the cells with PBS once and incubating at 37˚C for 10 minutes. Then PBS was removed and 200 µl dH_2O was added to each well and the plate was incubated at room temperature for 10 minutes to lyse the THP-1 cells. *B. ovis* cells were collected and serial diluted with a 10^{-1} dilution factor in PBS and plated on TSAB. Plates were incubated for 3 days and CFU were enumerated.

Phase contrast microscopy

Samples of *B. ovis* cells were grown on TSAB supplemented with kanamycin and incubated for 2 days. Cells were resuspended in milliQ H_2O and 1 µl of cells were spotted on an agarose pad on a cover slide

and imaged on a Leica DMI 6000 microscope in phase contrast with an HC PL APO 63x/1.4 numeric aperture (NA) oil Ph3 CS2 objective. Images were captured with an Orca-ER digital camera (Hamamatsu) controlled by Leica Application Suite X (Leica). Cell areas were measured from phase contrast images using BacStalk (65).

Cryo electron microscopy

B. ovis cells were grown on TSAB for 2 days and resuspended in PBS to a $OD_{600} \approx 1$. Five µl of cells were placed on a glow-discharged R 3.51 grid (Quantfoil), blotted for 3.5 s, air dried for 20 s, and plunged into liquid ethane using the Vitrobot robotic plunge freezer (Thermo). Samples were stored in liquid nitrogen before imaging. Cells were imaged on a ThermoScientific Talos Arctica Cryo-EM (Thermo) with a -10.00 µm defocus and 17,500x magnification. Images were captured with a Ceta camera (Thermo) with 2.0 s exposure time.

RNA extraction and sequencing

B. ovis strains were grown in Brucella broth at 37˚C in 5% CO_2 overnight. The next day, cultures were back diluted to OD_{600} = 0.05 in 12 ml Brucella broth and incubated on a rotor at 37˚C with 5% CO_2 for 7h. 9 ml of each culture was harvested by centrifugation, and the pellets were immediately resuspended in 1 ml TRIzol. Samples were stored at -80˚C until RNA extraction. To extract the RNA, samples were thawed and incubated at 65˚C for 10 minutes. 200 µl of chloroform was added to each sample and mixed by vortexing for 15 seconds. Samples were then incubated at room temperature for 5 minutes. Phases were separated by centrifugation at 17,000 x g for 15 minutes at 4˚C. The aqueous layer was transferred into a fresh tube. Sample was mixed with 500 µl of isopropanol and stored at -20˚C for 2h. After thawing, samples were centrifuged at 13,000 x g for 30 minutes at 4˚C. Supernatants were discarded and the pellets were washed with 1 ml of ice cold 70% ethanol. Samples were centrifuged at 13,000 x g at 4˚C for 5 minutes. Supernatants were discarded and pellets were air dried completely. Pellets were resuspended in 100 µl RNAse-free H_2O and incubated at 60˚C for 10 minutes. RNA samples were DNase treated using RNeasy Mini kit (Qiagen). RNA samples were sequenced at Microbial Genome Sequencing Center (Pittsburgh, PA) on an Illumina NextSeq 2000 (Illumina). RNA libraries for RNA-seq were prepared using Illumina Stranded RNA library preparation with RiboZero Plus rRNA depletion.

RNA-seq analysis

All RNA-seq analysis was conducted in CLC Genomics Workbench 21.0.4 (Qiagen). Reads were mapped to reference genome (*Brucella ovis* ATCC 25840, Genbank accessions NC_009504 and NC_009505). Differential expression for RNA-seq default settings were used to calculate the fold change of all annotated genes in mutant strains versus WT. Raw and processed RNA-seq data are publicly available in the NCBI GEO database at accession GSE229183.

ChIP DNA extraction and sequencing

To build the constructs for ChIP-seq analysis of strains expressing $CenR_{D55E}$ and $EssR_{D64E}$, regions containing each gene (including ~300 bp upstream) were PCR amplified from the *B. ovis* $cenR_{D55E}$ and $essR_{D64E}$ mutant strains with KOD polymerase. Amplified fragments were purified and inserted into plasmid pQF through restriction enzyme digestion and ligation to yield a 3xFLAG fusion at the 3' end of each gene. This C-terminal FLAG fusion plasmid construct was conjugated into *B. ovis* mutants using WM3064 as described above.

Cells were grown on TSAB plates supplemented with 30 µg/ml oxytetracycline for three days and resuspended in Brucella broth. Formaldehyde was added to a final concentration of 1% (w/v) to crosslink, and samples were incubated for 10 minutes on shaker. Crosslinker was quenched by adding 0.125 M glycine and was shaken for an additional 5 minutes. Cells were then centrifuged at 7,196 x g for 5 minutes at 4˚C and pellets were washed 4 times with cold PBS pH 7.5 and resuspended in 900 µl buffer [10 mM Tris pH 8, 1 mM EDTA, protease inhibitor cocktail tablet (Roche)]. 100 µl of 10 mg/ml lysozyme was added to each sample, which were then vortexed and incubated at 37˚C for 30 minutes before adding a final concentration of 0.1% SDS (w/v) to each sample. The samples were then

sonicated on ice for 15 cycles (20% magnitude, 20 seconds on/off) and centrifuged at 15,000xg for 10 minutes at 4˚C. Supernatants were collected, Triton X-100 was added to a concentration of 1%, and lysates were added to 30 µl SureBead Protein A magnetic agarose beads (BioRad) equlibrated with binding buffer [10 mM Tris pH 8, 1 mM EDTA pH8, 0.1% SDS, 1% Triton X-100] and incubated for 30 minutes at room temperature; this step has empirically improved signal for our FLAG IP protocols. Beads were collected on a magnetic stand, the supernatant was transferred to a fresh tube, and 5% of each sample supernatant was removed as the input DNA samples. 100 µl of α-FLAG magnetic agarose beads were then washed three times with binding buffer and incubated overnight at 4˚C shaking in 500 µl binding buffer plus 1% BSA to equilibrate the beads. The following day, α-FLAG beads were washed four times in binding buffer and cell lysates were added to the pre-washed beads and gently vortexed. Samples were incubated for 3h at room temperature with mixing and α-FLAG beads were collected on a magnetic stand and serially washed in 500 µl low-salt buffer [50 mM HEPES pH7.5, 1% Triton X-100, 150 mM NaCl], 500 µl high-salt buffer [50mM HEPES pH 7.5, 1% Triton X-100, 500 mM NaCl], and 500 µl LiCl buffer [10 mM Tris pH 8, 1 mM EDTA pH 8, 1% Triton X-100, 0.5% IGEPAL® CA-630, 150 mM LiCl]. To elute the protein-DNA complex bound to the beads, 100 µl elution buffer [10 mM Tris pH 8.0, 1 mM EDTA pH 8.0, 1% SDS, 100 ng/µl 3x FLAG peptide] was added to the beads and incubated at room temperature for 30 minutes with mixing. The eluate was collected, and the elution step was repeated. Input samples were brought to the same volume as output samples with elution buffer. For RNase A treatment, a final concentration of 300 mM NaCl and 100 µg/ml RNase A were added to each input and output sample and incubated at 37˚C for 30 minutes. Proteinase K was added to a final concentration of 200 µg/ml and the samples were incubated overnight at 65˚C to reverse crosslinks. ChIP DNA was purified with Zymo ChIP DNA Clean & Concentrator kit. The ChIP-seq library was prepared using Illumina DNA prep kit and IDT 10bp UDI indices; DNA samples were sequenced at SeqCenter (Pittsburgh, PA) on an Illumina Nextseq 2000.

ChIP-seq analysis

Output and input DNA sequences were first mapped to the reference genome (*Brucella ovis* ATCC 25840, Genbank accessions NC_009504 and NC_009505) in Galaxy using bowtie2 (66). ChIP-seq enriched peak calls from the mapping output data were carried out in Genrich (https://github.com/jsh58/Genrich) with parameters maximum q-value = 0.05, and minimum AUC (area under the curve) = 20; PCR duplicates were removed. bamCoverage (67) was used to create bigwig file tracks for each replicate, and peaks were visualized in IGB (68). Raw and processed ChIP-seq data are publicly available in the NCBI GEO database at accession GSE229183

Bacterial two hybrid β-galactosidase assay

The DNA fragments of the full-length, point mutant, and specific domains of *cenR* and *essR* were PCR amplified by KOD polymerase and cloned into split adenylyl cyclase plasmids (either pKT25 or pUT18c) (55) through restriction digestion and ligation. Each pair of pKT25 and pUT18c plasmids were co-transformed into chemically competent *E. coli* BTH101 cells. BTH101 strains carrying both pKT25 and pUT18c plasmids were grown in LB and incubated at 30˚C overnight while shaking. Fresh LB + 500 µM IPTG was inoculated with 100 µl of overnight culture and incubated at 30˚C until $OD_{600} \approx 0.3$-0.4. To assess two-hybrid interaction via reconstitution of adenylyl cyclase activity, 100 µl of culture was mixed with 100 µl chloroform and vortexed vigorously. 700 µl Z buffer (0.06 M Na_2HPO_4, 0.04 M NaH_2PO_4, 0.01 M KCl, 0.001 M $MgSO_4$) and 200 µl ortho-nitrophenyl- β-galactoside (ONPG) was added to each sample. The reactions were stopped with 1 ml of Na_2CO_3 after 7.8 minutes and colorimetric conversion of ONPG was measured at 420 nm (A_{420}) was measured. Miller Units were calculated as MU = A_{420} x 1000 / (OD_{600} x time x volume of cells).

Structure prediction

The heterodimeric structure of CenR and EssR was predicted using the protein complex prediction package AF2Complex (57), which utilizes the neural network models of AlphaFold2 (56). Computations were carried out on the Michigan State University high-performance computing cluster.

EssR-CenR co-immunoprecipitation assay

Strain construction, lysate production, and α-FLAG magnetic agarose beads preparation were the same as described above for ChIP-seq sample preparation. After preparation and centrifugation of the lysates, the supernatants were collected and 50 µl of each sample was mixed with equal amount of SDS loading buffer and stored at -20˚C. For FLAG IP, remaining lysates were applied to pre-washed α-FLAG beads and incubated at room temperature for 3h with shaking. Beads were washed and eluted as described above, eluate from each sample was incubated at 65˚C overnight to reverse crosslinking, and samples were then mixed with equal volume of SDS loading buffer. All samples collected were heated to 95˚C for 5 minutes before resolving on a 12% mini-PROTEAN precast gel (BioRad). A Western blot using polyclonal EssR antiserum was conducted following the protocol outlined in the Western blot method section below. The membrane was imaged using BioRad ChemiDoc Imaging System (BioRad).

Protein purification

DNA fragments that encode full length CenR and EssR, and EssS residues 191-488 (EssS for short) were PCR amplified by KOD polymerase and inserted into a pET23b-His6-SUMO expression vector through restriction digestion and ligation. Vectors were transformed into chemically competent *E. coli* BL21 Rosetta (DE3) / pLysS. All strains were grown in LB medium at 37˚C and induced with 0.5 mM isopropyl β-D-1-thiogalactopyranoside (IPTG) at $OD_{600} \approx 0.5$. Cell pellets were harvested after 2h of induction at 37˚C and stored at -80˚C until purification.

For protein purification, cell pellets were resuspended in 25 ml of lysis buffer (25 mM Tris pH8, 125 mM NaCl, 10 mM imidazole) with the addition of 1mM phenylmethylsulfonyl fluoride (PMSF) and 5 µg/ml DNase I. Samples were lysed through sonication on ice (20% magnitude, 20 seconds on/off) until the lysates were clear. Lysates were centrifuged, and the supernatant was added to 3 ml of Ni-nitrilotriacetic acid (NTA) superflow resin (Qiagen) and the mixture was applied onto a gravity drip column. The resin was washed with 20 ml of lysis buffer, 50 ml of wash buffer (25 mM Tris pH8, 150 mM NaCl, 30 mM imidazole) and the proteins were collected in 20 ml of elution buffer (25 mM Tris pH8, 150 mM NaCl, 300 mM imidazole) at 4˚C. For CenR and EssR, the elution was dialyzed and the His6-SUMO tags were cleaved with ubiquitin-like-specific protease 1 (Ulp1) overnight at 4˚C in dialysis buffer (25 mM Tris pH8, 150 mM NaCl). The next day, the digested protein was mixed with NTA superflow resin. The mixture was applied onto a gravity column and the purified and cleaved protein was collected from the flow through. His6-SUMO-EssS was dialyzed in dialysis buffer overnight at 4˚C and collected. All proteins were stored at 4˚C.

In vitro EssS-EssR phosphoryl transfer assay

Purified His-SUMO-EssS(191-488), CenR, and EssR were diluted to 5 µM with 1x kinase buffer (250 mM Tris pH8, 50 mM KCl, 10 mM $MgCl_2$, 10 mM $CaCl_2$, 1 mM DTT). 5 µl of ATP mix (4.5 µl 250 µM ATP, pH 7, 0.5 µl [32P]-ATP (10 µCi/µl) was added to 45 µl of 5 µM His-SUMO-EssS and the protein was allowed to autophosphorylate for 1h at room temperature. 5 µl of His-SUMO-EssS~P was mixed with 5 µl 1x kinase buffer and SDS loading buffer as the autophosphorylation control. To assess phosphoryl transfer, His-SUMO-EssS~P was mixed with equimolar of CenR, EssR, or a CenR/EssR mixture at various CenR:EssR molar ratios. Each phosphoryl transfer reaction was quenched with equal volume of SDS loading buffer. Reaction samples were loaded onto a 12% mini-PROTEAN precast gel (BioRad) and resolved at 180V at room temperature. The dye front of the gel was cut off and the rest of the gel was exposed to a phosphoscreen for 1-2h at room temperature. The phosphoscreen was imaged on a Typhoon phosphorimager (Cytiva), and gel band intensity was quantified using ImageQuant TL (Cytiva).

Western Blotting of EssR protein

B. ovis strains were grown on plain TSAB or TSAB supplemented with kanamycin for two days. Cells were collected and resuspended in sterile PBS to equivalent densities (measured optically at 600 nm). Cell resuspensions were mixed with an equal volume of SDS loading buffer and heated to 95˚C for 5

minutes. 10 µl of each sample was loaded onto a 12.5% SDS-PAGE gel and resolved at 180V at room temperature. The proteins were transferred to a PVDF membrane (Millipore) using a semi-dry transfer apparatus at 10V for 30 minutes at room temperature. The membrane was blocked in 20 ml Blotto (Tris-buffered saline Tween-20 (TBST) + 5% milk) for 1h at room temperature. The membrane was blocked in 10 ml Blott + polyclonal rabbit α-EssR antiserum (1:1,000 dilution), and the membrane was incubated for 1h at room temperature. The membrane was washed three times with TBST. Goat α-rabbit IgG poly-horseradish peroxidase secondary antibody (Invitrogen; 1:10,000 dilution) was added to 10 ml Blotto and the membrane was incubated for 1h at room temperature. The membrane was washed three times with TBST, developed with ProSignal Pico ECL Spray (Prometheus Protein Biology Products) and imaged on a BioRad ChemiDoc Imaging System. Bands were quantified using ImageLab Software (BioRad).

Acknowledgements
We thank Maeve McLaughlin for experimental guidance on ChIP-seq protocol and analysis, and current and former Crosson Lab members for helpful discussions over the course of this study. We also thank Sundharraman Subramanian at the Cryo-EM Facility at Michigan State University for assistance with Cryo-EM. This study was supported by NIH award R35GM131762 to S.C.

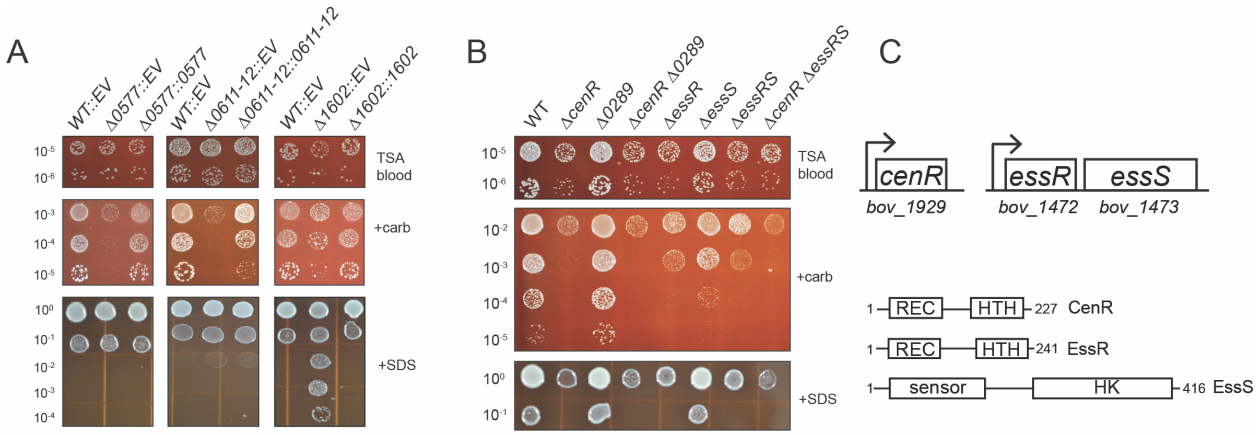

Figure 1: A comprehensive analysis of *B. ovis* TCS genes identified five genes/operons that contribute to carbenicillin and SDS resistance *in vitro*. (A) Strains harboring in-frame unmarked deletions (Δ) of *B. ovis* TCS gene loci *BOV_0577*, *BOV_0611-0612*, and *BOV_1602*, carrying *glmS*-integrated empty vectors (EV) or genetic complementation vectors (::locus number) were plated in $\log_{10}$ dilution series on plain TSAB (TSA blood agar) or TSAB containing 2 µg/ml carbenicillin (+carb) or 0.004% SDS (+SDS). (B) Strains harboring in-frame unmarked deletions (Δ) of *B. ovis* TCS gene loci *BOV_1929* (*cenR*), *BOV_0289*, *BOV_1472* (*essR*), *BOV_1473* (*essS*), alone and in combination plated as in panel A. Genetic complementation of panel B strains is shown in Figure S1. Dilution plating experiments were repeated at least three times for all strains, and one representative experiment is shown. (C) (top) Diagrams of the *cenR* and *essR-essS* genetic loci with *bov* gene locus numbers. (bottom) Protein domain models of CenR, EssR, and EssS with number of amino acid residues in each protein. REC is receiver domain; HTH is helix-turn-helix DNA binding domain, sensor is the predicted extracellular sensor domain, HK is histidine kinase domain.

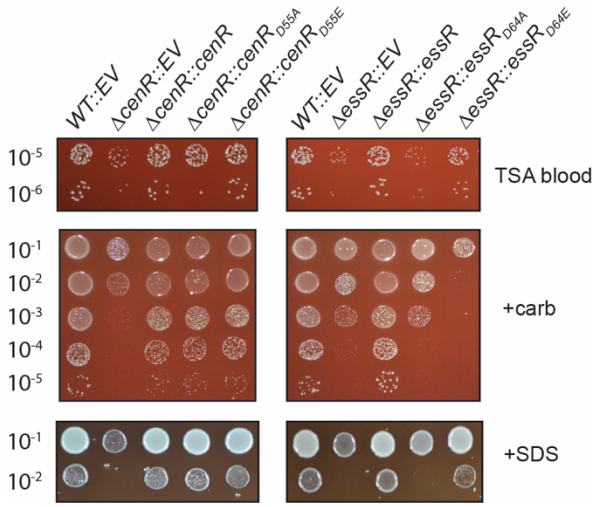

Figure 2: **Functional analysis of the conserved aspartyl phosphorylation sites of the CenR and EssR response regulators.** Test for genetic complementation of Δ*cenR* and Δ*essR* envelope stress phenotypes by expression of either non-phosphorylatable alleles of *cenR* (D55A) and *essR* (D64A) or putative phosphomimetic alleles (D55E / D64E). Conditions and dilution plating as in Figure 1; 2 µg/ml carbenicillin (+carb) and 0.004% SDS (+SDS). Δ*cenR* and Δ*essR* each carry an empty vector as control (EV). Experiments were repeated at least three times for all strains and one representative experiment is shown.

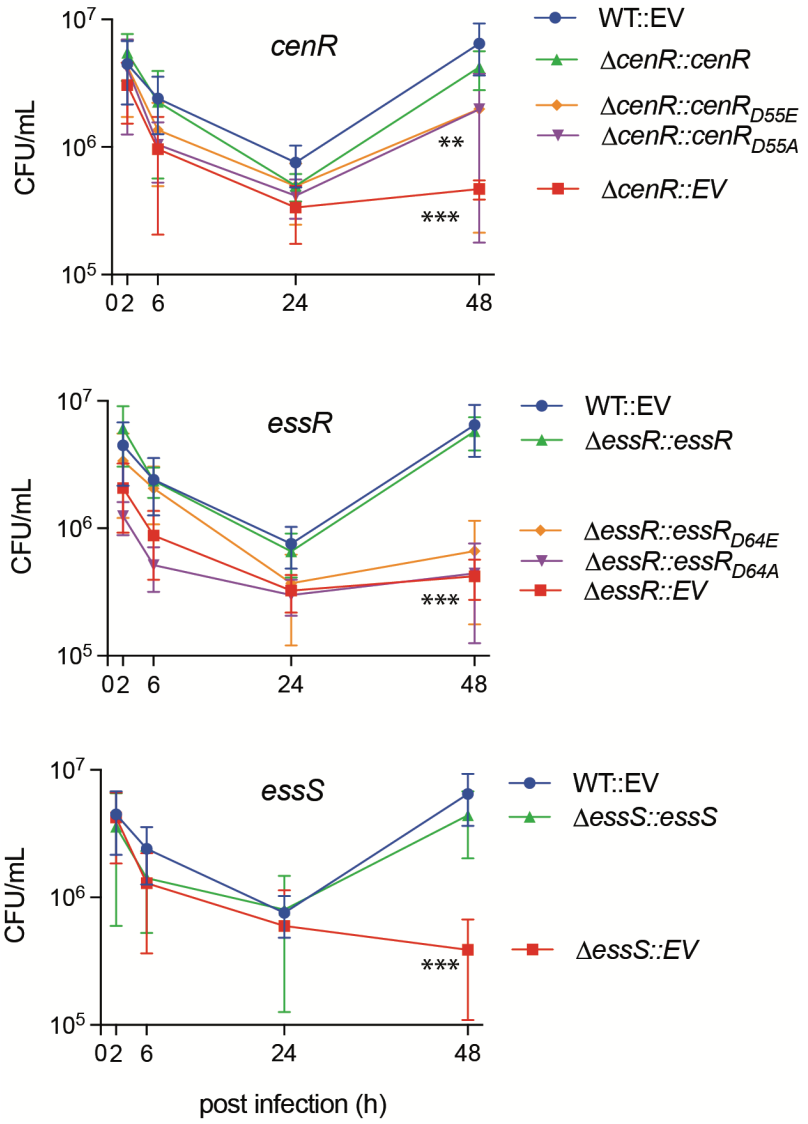

Figure 3: *B. ovis* Δ*cenR,* Δ*essR*, and Δ*essS* deletion strains have reduced fitness in the intracellular niche of mammalian macrophage-like cells; intact CenR and EssR aspartyl phosphorylation sites are important for protein function in the intracellular niche. Log_{10} colony forming units (CFU) per well of wild-type *B. ovis* carrying a *glmS*-integrated empty vector (WT::EV) (blue), Δ*cenR*, Δ*essR*, and Δ*essS* carrying the EV (red), or complementation of Δ*cenR*, Δ*essR*, and Δ*essS (*green) isolated from infected THP-1 cells and enumerated at 2, 6, 24 and 48 hours (h) post infection. The contribution of the conserved aspartyl phosphorylation sites of CenR and EssR to intracellular fitness was assessed by testing for genetic complementation of Δ*cenR* and Δ*essR* phenotypes by integration of either non-phosphorylatable alleles of *cenR* (D55A) and *essR* (D64A) (purple) or putative phosphomimetic alleles (D55E / D64E) (orange). Infections were repeated 3 times; error bars represent standard deviation of the three biological replicates. Statistical significance was calculated at 48h p.i. using one-way ANOVA, followed by Dunnett's multiple comparisons test to WT::EV control ($p < 0.001$, **; $p < 0.0001$, ***).

Figure 4: CenR and EssRS regulate an overlapping set of genes and have a correlated ChIP-seq profile. (A) Heat map of $\log_2$ fold change in gene expression in Δ*cenR* and Δ*essRS* deletion strains relative to wildtype (WT). Genes presented have a minimum fold change ≥ |2| (FDR p-value < 10^{-4}). Genes highlighted in orange are positioned adjacent on the chromosome and are potentially in operons. (B) EssR and CenR ChIP-seq peaks (q-value ≤ 0.05; minimum AUC = 20) along chromosomes 1 and 2. Red lines mark peaks that are shared CenR and EssR binding sites. Blue lines indicate peaks that are unique to either CenR or EssR.

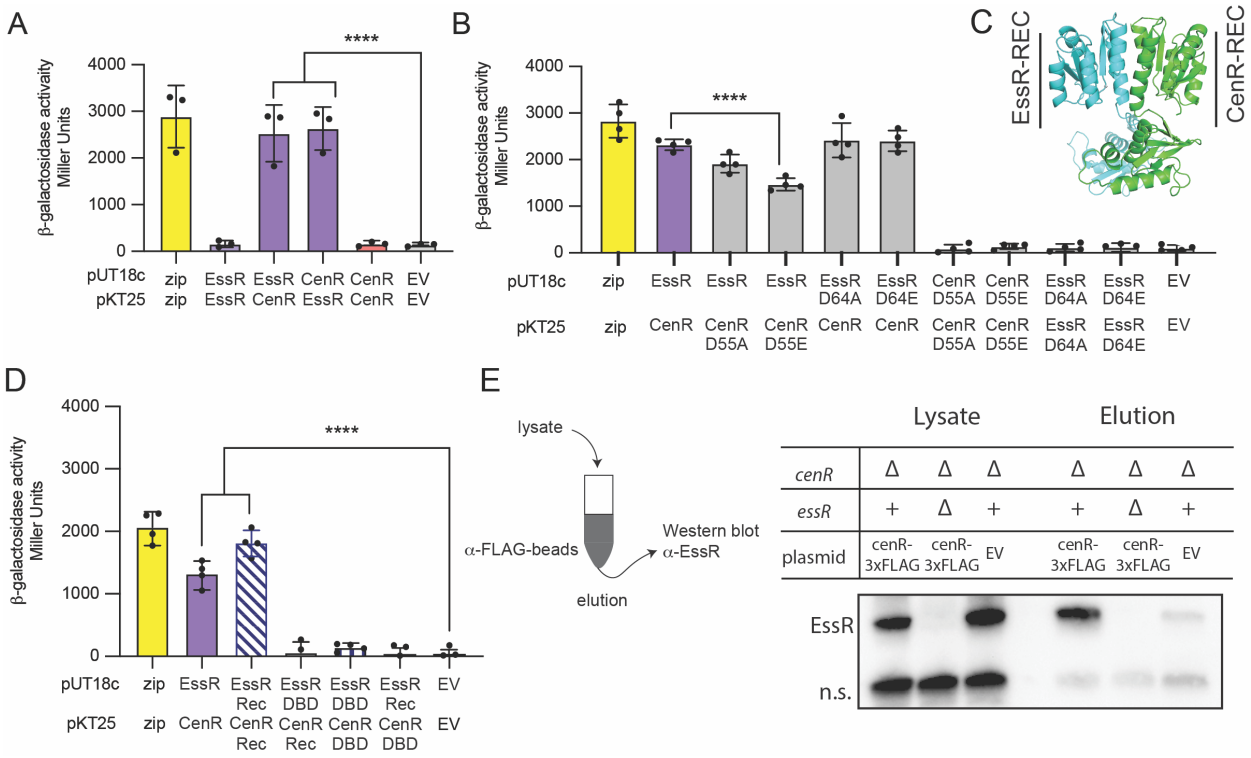

Figure 5: CenR and EssR physically interact in a heterologous system and in *B. ovis*. (A,B) Measurement of homomeric and heteromeric interactions between EssR and CenR (and their aspartyl phosphorylation site mutants; D→A & D→E) using an *E. coli* bacterial two-hybrid assay. Proteins were fused to split adenylate cyclase fragments in vectors pUT18c and pKT25. Positive control (zip) and empty vector (EV) negative controls are shown. (C) Predicted CenR:EssR heterodimer protein structure; CenR (green) and EssR (blue) (D) Test for interactions between DNA-binding domain (DBD) and receiver domain (Rec) fragments of EssR and CenR by bacterial two-hybrid. Error bars represent the standard deviation of 4 biological replicates. Statistical significance was calculated using one-way ANOVA, followed by Dunnett's multiple comparisons test ($p < 0.0005$, ***; $p < 0.0001$, ****) to EV control or WT CenR-EssR interaction. (E) Co-immunoprecipitation of EssR and CenR-3xFLAG from *B. ovis* lysate. (left) CenR-FLAG was captured using anti-FLAG beads, which were washed before elution. (right) EssR association with CenR-FLAG in the eluate was monitored by Western blot using polyclonal antiserum to EssR (α-EssR). Non-specific (n.s.) cross-reactive band is shown as an indicator of loading. Representative blot from three biological replicates.

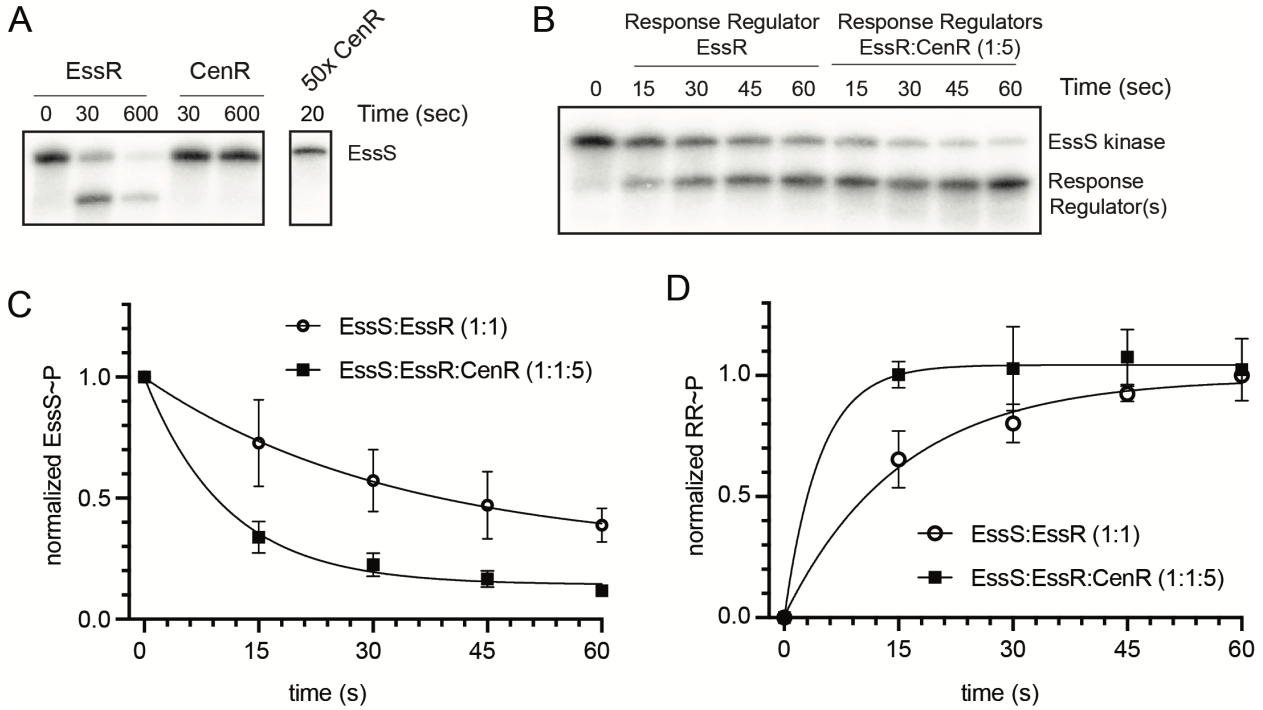

Figure 6: EssS specifically phosphorylates EssR; CenR stimulates phosphoryl transfer from EssS to EssR. (A) EssS autophosphorylation and phosphoryl transfer assay. Phosphoryl transfer from EssS to either EssR or CenR was assessed at 30s and 600s timepoints. 50x molar excess of CenR was added to phospho-EssS to test kinase specificity. Lower molecular weight band corresponds to phospho-EssR. B) Phosphoryl transfer kinetics from EssS to EssR at a 1:1 molar ratio and at a 1:1:5 (EssS:EssR:CenR) molar ratio. C) Normalized EssS-P dephosphorylation kinetics at a 1:1 molar ratio of EssS to EssR and at a 1:1:5 (EssS:EssR:CenR) ratio. D) Normalized EssR phosphorylation kinetics at the same molar ratios as panel C. Points and error bars represent the mean ± standard deviation of three replicates.

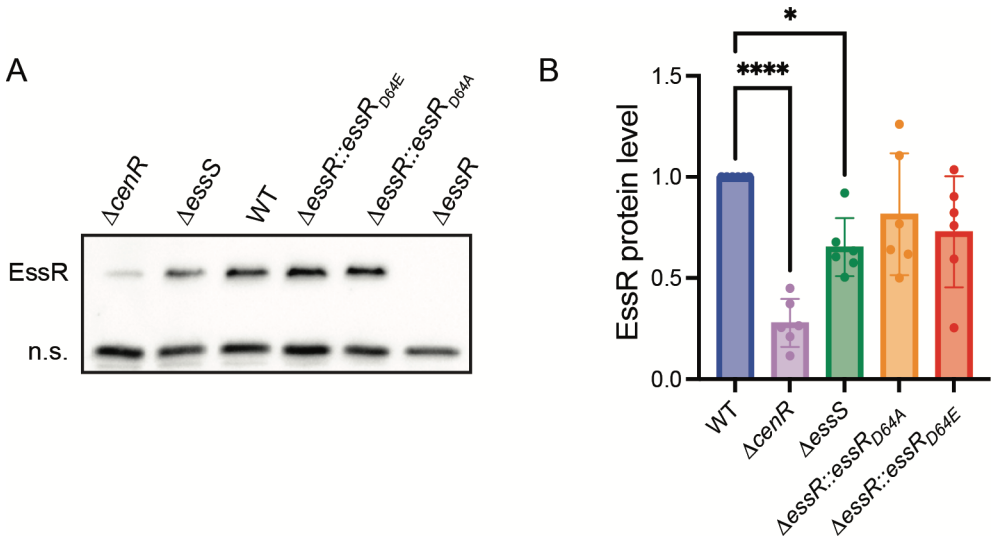

Figure 7: Steady state levels of EssR are influenced by *cenR* and *essS*. A) α-EssR Western blot of lysate from WT *B. ovis* and *B. ovis* expressing EssR(D64A), EssR(D64E), and in strains lacking *essS* (Δ*essS*), *cenR* (Δ*cenR*) or *essR (*Δ*essR*). B) Quantification of normalized EssR band intensities from six independent replicate blots. Mean EssR intensity from WT cells is set to 1; the relative EssR level in other strains is plotted. Error bars represent the mean ± standard deviation of the six replicates. Statistical significance was calculated using one-way ANOVA, followed by Dunnett's multiple comparisons test to WT ($p < 0.05$, *; $p < 0.0001$, ****).

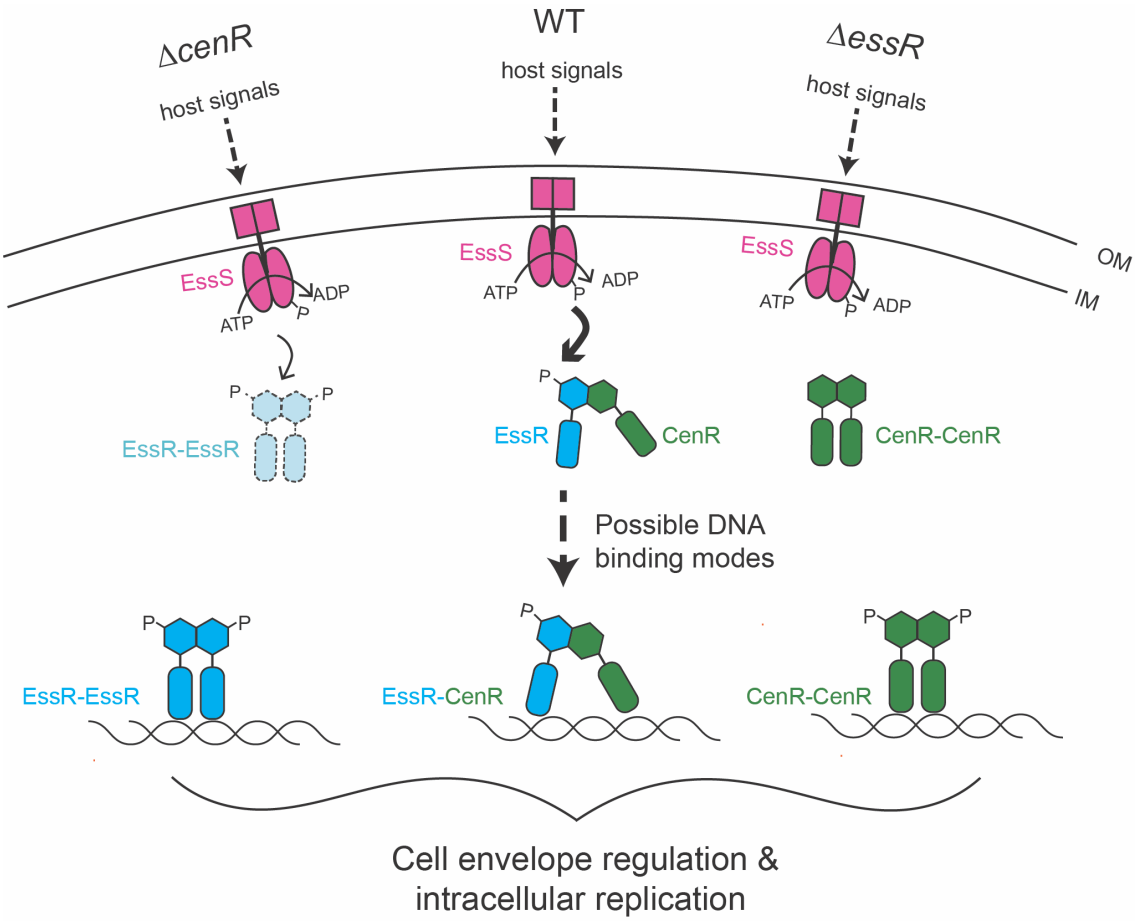

Figure 8: Model of EssS-EssR-CenR-dependent gene regulation in *B. ovis*. Upon detection of host signals, EssS (pink) autophosphorylates and transfers a phosphoryl group (P) to EssR (blue). CenR (green) supports EssS-EssR signal transduction by directly stimulating phosphoryl transfer from EssS and EssR via a receiver domain interaction. Loss of CenR results in diminished EssR levels (lighter blue with dashed outlines), providing evidence that the CenR-EssR interaction supports stability of EssR in the cell. CenR and EssR directly interact with an overlapping set of promoters, and three possible modes of transcriptional regulation by EssR and CenR are shown: EssR-EssR homodimer, EssR-CenR heterodimer, and/or CenR-CenR homodimers binding to target promoters. Genes regulated by the EssS-EssR-CenR system contribute to *B. ovis* growth/survival during cell envelope stress *in vitro*, and support intracellular replication in a macrophage infection model.

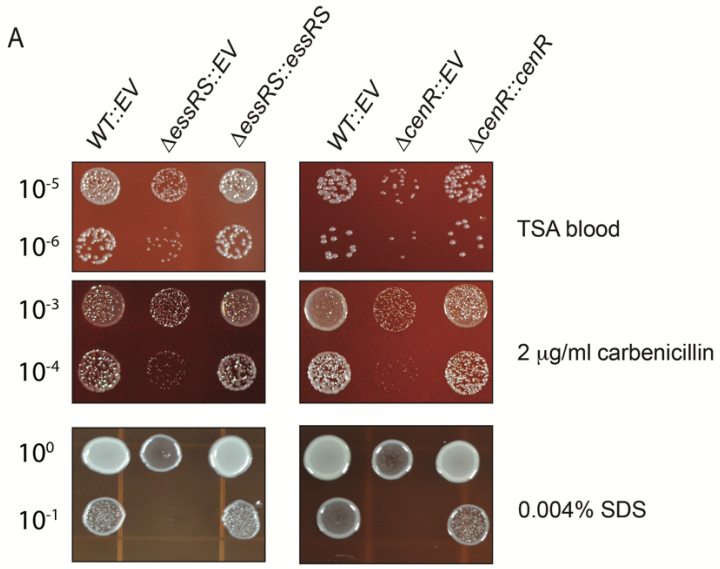

B

```
CenR  6    ILIVDDDEDLRSILVEQLELCEEFQILQEDSAGKGIQTARNGIVDLLIMDVGLPDMDGRE  65
           +L+VDDD  +RS+L + L     F++    SA +  +       DLLI+DV +P   G
EssR  16   LLVVDDDTRIRSLLSQYL-TNSGFRVTMAGSAAEARRKLEGIDFDLLILDVMMPGETGVS  74

CenR  66   AVKLLRKGGFKAPIIMLTGHDTESDTILGLESGANDYVTKPFKFAVLLARVRAQLRQ---  122
             + LR+     PI+MLT        I GL +GA+DY+ KPF    L  R+   LR+
EssR  75   LTRSLREQK-NVPILMLTALSETDSRIDGLAAGADDYLPKPFDPRELTLRINNILRRGAP  133

CenR  123  HEQSEDATFIVGPYTFKPGQKLLIDEKGSK-IRLTEKEAAIIKYLYRAGDKVIGRDVLLE  181
             Q +    + GPYTF   ++ L  +KG++ I+LT++E  I+        + I R
EssR  134  PAQPKIEQIVFGPYTFFIPRREL--KKGTETIKLTDREQDIMAIFAERAGETIPR----H  187

CenR  182  EVWGYNSGVTTHTLETHVYRLRQKIEKDPSNATLLVTESG-GYKL  225
           E+ G +  V   T++  + RLR+KIE+DP+N   L T  G GYKL
EssR  188  ELTGQDGDVGERTIDVQINRLRRKIEQDPANPVWLQTVRGIGYKL  232
```

Figure S1. *Genetic complementation of Δ*essRS* and Δ*cenR* mutants and CenR-EssR alignment. (A) Genetic complementation Δ*essRS* and Δ*cenR* carbenicillin and SDS plate phenotypes by Tn7 integration of vectors expressing *essRS* or *cenR* into the *glmS* locus. Dilution plating experiments were repeated at least three times for all strains. One representative experiment is shown. (B) Amino acid sequence alignment of CenR and EssR. Area highlighted in yellow shows the protein-protein interaction interface predicted by AFComplex2 (see Figure 5C).

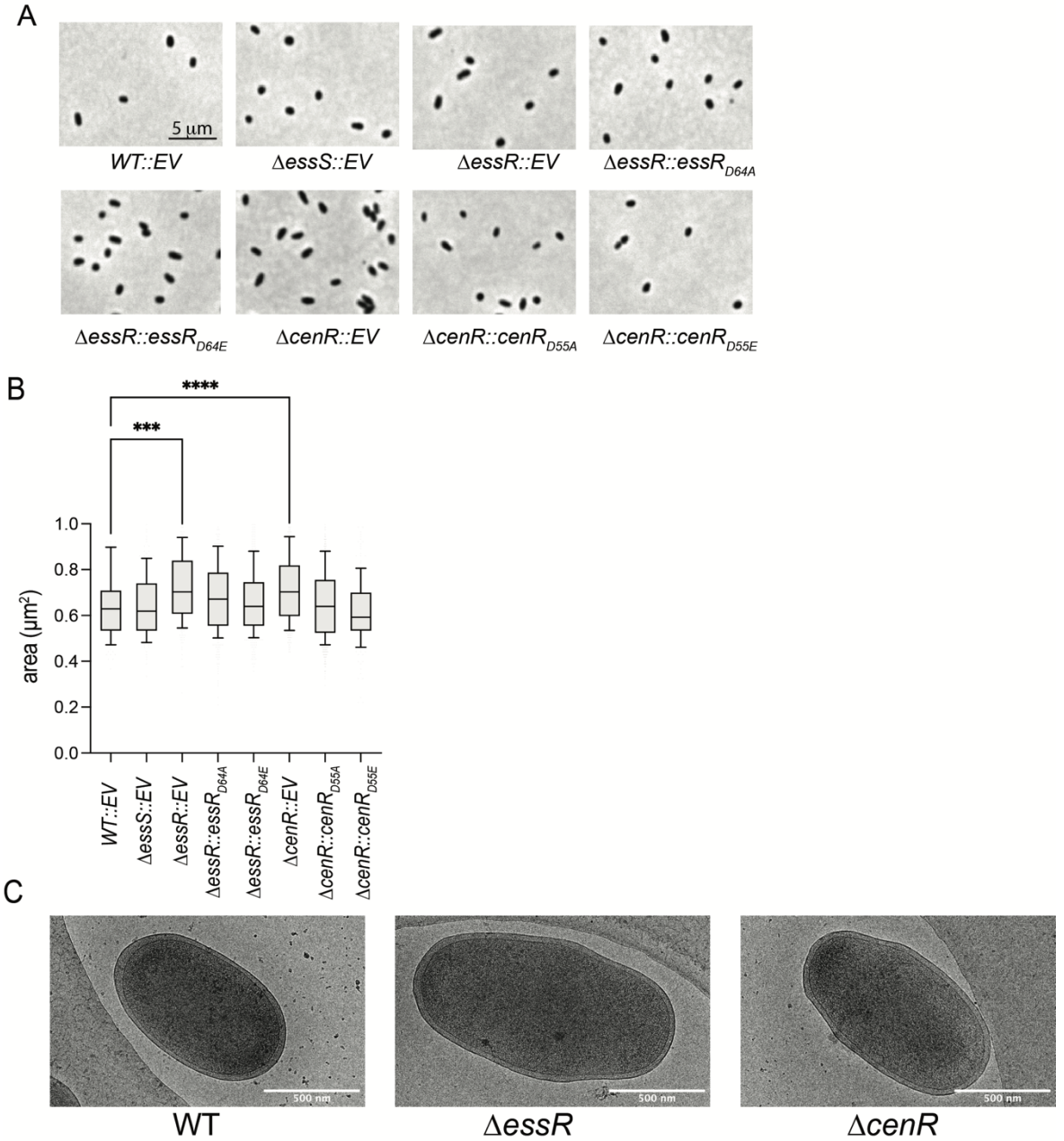

Figure S2: Deletion of *cenR* and *essR* results in increased cell area. A) Phase-contrast micrographs (630x magnification) of WT *B. ovis*, Δ*essS*, Δ*essR*, and Δ*cenR* in-frame deletion mutants; Δ*essR* complemented with *essR*$_{D64A}$ and *essR*$_{D64E}$; Δ*cenR* complemented with *cenR*$_{D55A}$ and cen*R*$_{D55E}$. B) Cell area analysis of WT (n=113), Δ*essS* (n=173), Δ*essR* (n=242), and Δ*cenR* (n=535) empty vector control strains (EV), Δ*essR* complemented with *essR*$_{D64A}$ (n=478) and *essR*$_{D64E}$ (n=466) alleles and Δ*cenR* complemented with *cenR*$_{D55A}$ (n=908) and cen*R*$_{D55E}$ (n=180) alleles. Mean is shown as a horizontal line in the box (25th-75th percentile); whiskers capture from 10th-90th percentile. Statistical significance was calculated using one-way ANOVA, followed by Dunnett's multiple comparison test to WT empty vector control (WT::EV) ($p < 0.001$, ***; $p < 0.0001$, ****). C) Representative cryo-EM images of WT *B. ovis*, Δ*essR*, and Δ*cenR* in-frame deletion mutants.

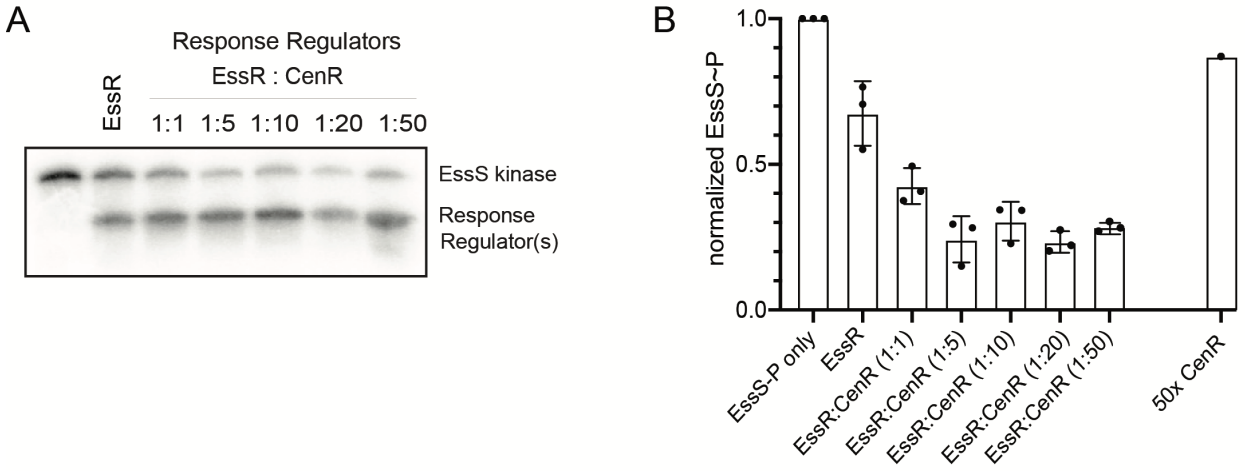

Figure S3. CenR enhances dephosphorylation of EssS~P in the presence of EssR. A) *In vitro* phosphoryl transfer assay with purified EssS kinase domain and EssR (1:1) and increasing ratiometric amounts of CenR. All reactions were stopped after 20s. B) Quantification of EssS~P levels; mean EssS~P band intensity is set to 1 in the EssS~P only reaction. Normalized EssS~P levels 20s after addition of EssR and CenR in varying ratios is plotted. Error bars represent the standard deviation of three biological replicates.

References

1. Battesti A, Majdalani N, Gottesman S. 2011. The RpoS-mediated general stress response in Escherichia coli. Annu Rev Microbiol 65:189-213. PMC7356644.
2. Fiebig A, Herrou J, Willett J, Crosson S. 2015. General Stress Signaling in the Alphaproteobacteria. Annu Rev Genet 49:603-25. PMC4710059.
3. Flores-Kim J, Darwin AJ. 2016. The Phage Shock Protein Response. Annu Rev Microbiol 70:83-101.
4. Hecker M, Pane-Farre J, Volker U. 2007. SigB-dependent general stress response in Bacillus subtilis and related gram-positive bacteria. Annu Rev Microbiol 61:215-36.
5. Kenney LJ. 2019. The role of acid stress in Salmonella pathogenesis. Curr Opin Microbiol 47:45-51.
6. Ruhland BR, Reniere ML. 2019. Sense and sensor ability: redox-responsive regulators in Listeria monocytogenes. Curr Opin Microbiol 47:20-25. PMC6502700.
7. Kim HS, Caswell CC, Foreman R, Roop RM, 2nd, Crosson S. 2013. The Brucella abortus general stress response system regulates chronic mammalian infection and is controlled by phosphorylation and proteolysis. J Biol Chem 288:13906-16. PMC3650426.
8. Kim HS, Willett JW, Jain-Gupta N, Fiebig A, Crosson S. 2014. The Brucella abortus virulence regulator, LovhK, is a sensor kinase in the general stress response signalling pathway. Mol Microbiol 94:913-25. PMC4227936.
9. Manterola L, Guzman-Verri C, Chaves-Olarte E, Barquero-Calvo E, de Miguel MJ, Moriyon I, Grillo MJ, Lopez-Goni I, Moreno E. 2007. BvrR/BvrS-controlled outer membrane proteins Omp3a and Omp3b are not essential for Brucella abortus virulence. Infect Immun 75:4867-74. PMC2044513.
10. Elzer PH, Phillips RW, Robertson GT, Roop RM, 2nd. 1996. The HtrA stress response protease contributes to resistance of Brucella abortus to killing by murine phagocytes. Infect Immun 64:4838-41. PMC174454.
11. Abdou E, Deredjian A, Jimenez de Bagues MP, Kohler S, Jubier-Maurin V. 2013. RegA, the regulator of the two-component system RegB/RegA of Brucella suis, is a controller of both oxidative respiration and denitrification required for chronic infection in mice. Infect Immun 81:2053-61. PMC3676001.
12. Occhialini A, Jimenez de Bagues MP, Saadeh B, Bastianelli D, Hanna N, De Biase D, Kohler S. 2012. The glutamic acid decarboxylase system of the new species Brucella microti contributes to its acid resistance and to oral infection of mice. J Infect Dis 206:1424-32.
13. Budnick JA, Sheehan LM, Colquhoun JM, Dunman PM, Walker GC, Roop RM, 2nd, Caswell CC. 2018. Endoribonuclease YbeY Is Linked to Proper Cellular Morphology and Virulence in Brucella abortus. J Bacteriol 200. PMC5971472.
14. Herrou J, Willett JW, Fiebig A, Czyz DM, Cheng JX, Ultee E, Briegel A, Bigelow L, Babnigg G, Kim Y, Crosson S. 2019. Brucella Periplasmic Protein EipB Is a Molecular Determinant of Cell Envelope Integrity and Virulence. J Bacteriol 201. PMC6531618.
15. Herrou J, Willett JW, Fiebig A, Varesio LM, Czyz DM, Cheng JX, Ultee E, Briegel A, Bigelow L, Babnigg G, Kim Y, Crosson S. 2019. Periplasmic protein EipA determines envelope stress resistance and virulence in Brucella abortus. Mol Microbiol 111:637-661. PMC6417958.
16. Steele KH, Baumgartner JE, Valderas MW, Roop RM, 2nd. 2010. Comparative study of the roles of AhpC and KatE as respiratory antioxidants in Brucella abortus 2308. J Bacteriol 192:4912-22. PMC2944529.
17. Robertson GT, Kovach ME, Allen CA, Ficht TA, Roop RM, 2nd. 2000. The Brucella abortus Lon functions as a generalized stress response protease and is required for wild-type virulence in BALB/c mice. Mol Microbiol 35:577-88.
18. Roop RM, 2nd, Barton IS, Hopersberger D, Martin DW. 2021. Uncovering the Hidden Credentials of Brucella Virulence. Microbiol Mol Biol Rev 85. PMC8549849.
19. Alakavuklar M, Fiebig A, Crosson S. 2023. The Brucella cell envelope. Annu Rev Microbiol in press.

20. Laub MT, Goulian M. 2007. Specificity in two-component signal transduction pathways. Annu Rev Genet 41:121-45.
21. Mike LA, Choby JE, Brinkman PR, Olive LQ, Dutter BF, Ivan SJ, Gibbs CM, Sulikowski GA, Stauff DL, Skaar EP. 2014. Two-component system cross-regulation integrates Bacillus anthracis response to heme and cell envelope stress. PLoS Pathog 10:e1004044. PMC3968170.
22. Noriega CE, Lin HY, Chen LL, Williams SB, Stewart V. 2010. Asymmetric cross-regulation between the nitrate-responsive NarX-NarL and NarQ-NarP two-component regulatory systems from Escherichia coli K-12. Mol Microbiol 75:394-412. PMC3034140.
23. Reyes Ruiz LM, Fiebig A, Crosson S. 2019. Regulation of bacterial surface attachment by a network of sensory transduction proteins. PLoS Genet 15:e1008022. PMC6530869.
24. Stewart V, Bledsoe PJ. 2003. Synthetic lac operator substitutions for studying the nitrate- and nitrite-responsive NarX-NarL and NarQ-NarP two-component regulatory systems of Escherichia coli K-12. J Bacteriol 185:2104-11. PMC151514.
25. Howell A, Dubrac S, Noone D, Varughese KI, Devine K. 2006. Interactions between the YycFG and PhoPR two-component systems in Bacillus subtilis: the PhoR kinase phosphorylates the non-cognate YycF response regulator upon phosphate limitation. Mol Microbiol 59:1199-215.
26. Matsubara M, Kitaoka SI, Takeda SI, Mizuno T. 2000. Tuning of the porin expression under anaerobic growth conditions by his-to-Asp cross-phosphorelay through both the EnvZ-osmosensor and ArcB-anaerosensor in Escherichia coli. Genes Cells 5:555-69.
27. Salvail H, Groisman EA. 2020. The phosphorelay BarA/SirA activates the non-cognate regulator RcsB in Salmonella enterica. PLoS Genet 16:e1008722. PMC7241856.
28. Radeck J, Fritz G, Mascher T. 2017. The cell envelope stress response of Bacillus subtilis: from static signaling devices to dynamic regulatory network. Curr Genet 63:79-90.
29. Saha S, Lach SR, Konovalova A. 2021. Homeostasis of the Gram-negative cell envelope. Curr Opin Microbiol 61:99-106. PMC8577651.
30. Silhavy TJ, Kahne D, Walker S. 2010. The bacterial cell envelope. Cold Spring Harb Perspect Biol 2:a000414. PMC2857177.
31. Stranahan LW, Arenas-Gamboa AM. 2021. When the Going Gets Rough: The Significance of Brucella Lipopolysaccharide Phenotype in Host-Pathogen Interactions. Front Microbiol 12:713157. PMC8319746.
32. Bensig EO, Valadez-Cano C, Kuang Z, Freire IR, Reyes-Prieto A, MacLellan SR. 2022. The two-component regulatory system CenK-CenR regulates expression of a previously uncharacterized protein required for salinity and oxidative stress tolerance in Sinorhizobium meliloti. Front Microbiol 13:1020932. PMC9561847.
33. Lakey BD, Myers KS, Alberge F, Mettert EL, Kiley PJ, Noguera DR, Donohue TJ. 2022. The essential Rhodobacter sphaeroides CenKR two-component system regulates cell division and envelope biosynthesis. PLoS Genet 18:e1010270. PMC9275681.
34. Skerker JM, Prasol MS, Perchuk BS, Biondi EG, Laub MT. 2005. Two-component signal transduction pathways regulating growth and cell cycle progression in a bacterium: a system-level analysis. PLoS Biol 3:e334. PMC1233412.
35. Sternon JF, Godessart P, Goncalves de Freitas R, Van der Henst M, Poncin K, Francis N, Willemart K, Christen M, Christen B, Letesson JJ, De Bolle X. 2018. Transposon Sequencing of Brucella abortus Uncovers Essential Genes for Growth In Vitro and Inside Macrophages. Infect Immun 86. PMC6056880.
36. Chen E, Alakavuklar M, Fiebig A, Crosson S. 2022. Brucella ovis Tn-himar sequencing dataset, NCBI Sequence Read Archive.
37. DeJesus MA, Ambadipudi C, Baker R, Sassetti C, Ioerger TR. 2015. TRANSIT--A Software Tool for Himar1 TnSeq Analysis. PLoS Comput Biol 11:e1004401. PMC4598096.
38. De Bolle X, Crosson S, Matroule JY, Letesson JJ. 2015. Brucella abortus Cell Cycle and Infection Are Coordinated. Trends Microbiol 23:812-821. PMC8800490.

39. Guzman-Verri C, Manterola L, Sola-Landa A, Parra A, Cloeckaert A, Garin J, Gorvel JP, Moriyon I, Moreno E, Lopez-Goni I. 2002. The two-component system BvrR/BvrS essential for Brucella abortus virulence regulates the expression of outer membrane proteins with counterparts in members of the Rhizobiaceae. Proc Natl Acad Sci U S A 99:12375-80. PMC129452.
40. Martin-Martin AI, Sancho P, de Miguel MJ, Fernandez-Lago L, Vizcaino N. 2012. Quorum-sensing and BvrR/BvrS regulation, the type IV secretion system, cyclic glucans, and BacA in the virulence of Brucella ovis: similarities to and differences from smooth brucellae. Infect Immun 80:1783-93. PMC3347429.
41. Sola-Landa A, Pizarro-Cerda J, Grillo MJ, Moreno E, Moriyon I, Blasco JM, Gorvel JP, Lopez-Goni I. 1998. A two-component regulatory system playing a critical role in plant pathogens and endosymbionts is present in Brucella abortus and controls cell invasion and virulence. Mol Microbiol 29:125-38.
42. Stein BJ, Fiebig A, Crosson S. 2021. The ChvG-ChvI and NtrY-NtrX Two-Component Systems Coordinately Regulate Growth of Caulobacter crescentus. J Bacteriol 203:e0019921. PMC8351639.
43. Herrou J, Crosson S, Fiebig A. 2017. Structure and function of HWE/HisKA2-family sensor histidine kinases. Curr Opin Microbiol 36:47-54. PMC5534388.
44. Henry JT, Crosson S. 2011. Ligand-binding PAS domains in a genomic, cellular, and structural context. Annu Rev Microbiol 65:261-86. PMC3298442.
45. Gourley CR, Petersen E, Harms J, Splitter G. 2015. Decreased in vivo virulence and altered gene expression by a Brucella melitensis light-sensing histidine kinase mutant. Pathog Dis 73:1-8. PMC4310819.
46. Liu W, Dong H, Liu W, Gao X, Zhang C, Wu Q. 2012. OtpR regulated the growth, cell morphology of B. melitensis and tolerance to beta-lactam agents. Vet Microbiol 159:90-8.
47. Liu W, Dong H, Li J, Ou Q, Lv Y, Wang X, Xiang Z, He Y, Wu Q. 2015. RNA-seq reveals the critical role of OtpR in regulating Brucella melitensis metabolism and virulence under acidic stress. Sci Rep 5:10864. PMC4542472.
48. Zhang X, Ren J, Li N, Liu W, Wu Q. 2009. Disruption of the BMEI0066 gene attenuates the virulence of Brucella melitensis and decreases its stress tolerance. Int J Biol Sci 5:570-7. PMC2737717.
49. Parsons JD, Cocker CR, East AK, Wheatley RM, Ramachandran VK, Kaschani F, Kaiser M, Poole PS. 2022. Factors governing attachment of *Rhizobium leguminosarum* to legume roots. BioRxiv https://doi.org/10.1101/2022.11.21.517457.
50. Marchler-Bauer A, Zheng C, Chitsaz F, Derbyshire MK, Geer LY, Geer RC, Gonzales NR, Gwadz M, Hurwitz DI, Lanczycki CJ, Lu F, Lu S, Marchler GH, Song JS, Thanki N, Yamashita RA, Zhang D, Bryant SH. 2013. CDD: conserved domains and protein three-dimensional structure. Nucleic Acids Res 41:D348-52. PMC3531192.
51. Kenney LJ, Anand GS. 2020. EnvZ/OmpR Two-Component Signaling: An Archetype System That Can Function Noncanonically. EcoSal Plus 9. PMC7192543.
52. Vogt SL, Raivio TL. 2012. Just scratching the surface: an expanding view of the Cpx envelope stress response. FEMS Microbiol Lett 326:2-11.
53. Kleinman CL, Sycz G, Bonomi HR, Rodriguez RM, Zorreguieta A, Sieira R. 2017. ChIP-seq analysis of the LuxR-type regulator VjbR reveals novel insights into the Brucella virulence gene expression network. Nucleic Acids Res 45:5757-5769. PMC5449634.
54. Hallez R, Mignolet J, Van Mullem V, Wery M, Vandenhaute J, Letesson JJ, Jacobs-Wagner C, De Bolle X. 2007. The asymmetric distribution of the essential histidine kinase PdhS indicates a differentiation event in Brucella abortus. EMBO J 26:1444-55. PMC1817626.
55. Karimova G, Ullmann A, Ladant D. 2000. A bacterial two-hybrid system that exploits a cAMP signaling cascade in Escherichia coli. Methods Enzymol 328:59-73.
56. Jumper J, Evans R, Pritzel A, Green T, Figurnov M, Ronneberger O, Tunyasuvunakool K, Bates R, Zidek A, Potapenko A, Bridgland A, Meyer C, Kohl SAA, Ballard AJ, Cowie A, Romera-Paredes B, Nikolov S, Jain R, Adler J, Back T, Petersen S, Reiman D, Clancy E,

Zielinski M, Steinegger M, Pacholska M, Berghammer T, Bodenstein S, Silver D, Vinyals O, Senior AW, Kavukcuoglu K, Kohli P, Hassabis D. 2021. Highly accurate protein structure prediction with AlphaFold. Nature 596:583-589. PMC8371605.
57. Gao M, Nakajima An D, Parks JM, Skolnick J. 2022. AF2Complex predicts direct physical interactions in multimeric proteins with deep learning. Nat Commun 13:1744. PMC8975832.
58. Cardona ST, Choy M, Hogan AM. 2018. Essential Two-Component Systems Regulating Cell Envelope Functions: Opportunities for Novel Antibiotic Therapies. J Membr Biol 251:75-89.
59. Macritchie DM, Raivio TL. 2009. Envelope Stress Responses. EcoSal Plus 3.
60. Stewart V. 2003. Biochemical Society Special Lecture. Nitrate- and nitrite-responsive sensors NarX and NarQ of proteobacteria. Biochem Soc Trans 31:1-10.
61. Al-Bassam MM, Bibb MJ, Bush MJ, Chandra G, Buttner MJ. 2014. Response regulator heterodimer formation controls a key stage in Streptomyces development. PLoS Genet 10:e1004554. PMC4125116.
62. Castanie-Cornet MP, Cam K, Bastiat B, Cros A, Bordes P, Gutierrez C. 2010. Acid stress response in Escherichia coli: mechanism of regulation of gadA transcription by RcsB and GadE. Nucleic Acids Res 38:3546-54. PMC2887963.
63. Venkatesh GR, Kembou Koungni FC, Paukner A, Stratmann T, Blissenbach B, Schnetz K. 2010. BglJ-RcsB heterodimers relieve repression of the Escherichia coli bgl operon by H-NS. J Bacteriol 192:6456-64. PMC3008536.
64. Wetmore KM, Price MN, Waters RJ, Lamson JS, He J, Hoover CA, Blow MJ, Bristow J, Butland G, Arkin AP, Deutschbauer A. 2015. Rapid quantification of mutant fitness in diverse bacteria by sequencing randomly bar-coded transposons. mBio 6:e00306-15. PMC4436071.
65. Hartmann R, van Teeseling MCF, Thanbichler M, Drescher K. 2020. BacStalk: A comprehensive and interactive image analysis software tool for bacterial cell biology. Mol Microbiol 114:140-150.
66. Langmead B, Salzberg SL. 2012. Fast gapped-read alignment with Bowtie 2. Nat Methods 9:357-9. PMC3322381.
67. Ramirez F, Ryan DP, Gruning B, Bhardwaj V, Kilpert F, Richter AS, Heyne S, Dundar F, Manke T. 2016. deepTools2: a next generation web server for deep-sequencing data analysis. Nucleic Acids Res 44:W160-5. PMC4987876.
68. Freese NH, Norris DC, Loraine AE. 2016. Integrated genome browser: visual analytics platform for genomics. Bioinformatics 32:2089-95. PMC4937187.